AFIT/GNE/ENP/92J-01

NEUTRON FLUENCE AND DOSE FROM A VARIAN CLINAC 1800 ACCELERATOR

THESIS

Richard A. Jackson
Captain, USAF

AFIT/GNE/ENP/92J-01

AFIT/GNE/ENP/92J-01

NEUTRON FLUENCE AND DOSE FROM A VARIAN CLINAC 1800 ACCELERATOR

THESIS

Presented to the Faculty of the School of Engineering
of the Air Force Institue of Technology
Air University
in Partial Fulfillment of the
Requirements for the Degree of
Master of Science in Nuclear Science

Richard A. Jackson
Captain, USAF

November 1991

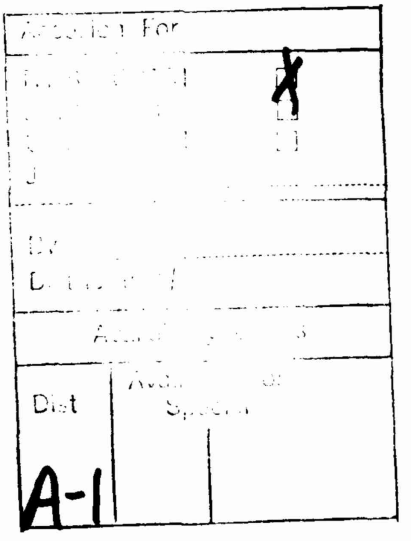

Preface

The aim of this study was the measurement of neutrons from the high-energy x-ray machine used for cancer therapy at the Wright-Patterson Air Force Base Medical Center. Thin gold foils inserted into flux integrators (polyethylene cylinders) were used to measure the neutron output from the x-ray machine and the results reported. To ensure the validity of these neutron measurements, a series of calibration experiments were done on various parts of the detection and counting system; these are also reported.

This document is the culmination of a long struggle on the part of myself, the author. Of course I wish tc acknowledge the contributions by my major professor, Dr. George John. The idea for this study was his, and I am grateful for his forbearance in dealing with this recalcitrant student. I wish also to thank Capt Ken Wohlt, medical physicist at the WPAFB Medical Center, without whose help I could never have done the actual neutron measurements on the x-ray machine. Let me not forget also the friends who gave me encouragement to complete this work. Most importantly I thank all those family, friends, peers, teachers, preachers, counselors, and others who believed in me during my formative years and beyond. They gave me the confidence and strength to believe in myself, so that I was not totally discouraged by the skepticism of others. I dedicate this effort to those who saw the potential in me and encouraged me to live up to it. I also dedicate it to all who struggle through adversity, yet persevere to finish the task. To them belongs the final victory as only they can know it.

Richard A. Jackson

Table of Contents

List of Figures

List of Tables

Abstract

The goals of this study were (1) to verify calibration factors determined by previous experiment for relating counts from activated gold foils to neutron fluences, and (2) to use the method to determine neutron fluences under various operating conditions of the Varian Clinac 1800 (18-MeV) electron accelerator at the WPAFB Medical Center. For comparison similar measurements were made of the CGM Saturne 1 at Kettering Memorial Hospital, Dayton, Ohio.

Cadmium-difference pairs in a standard graphite pile were employed to verify the counting efficiency of the Geiger-Mueller beta counting system used to count the foil activity. They were also used to determine the relation between the thickness of the gold foils and the activity induced in the foil (self shielding and self absorption).

A PuBe neutron source was used to calibrate the response of flux integrators in which gold foils are activated by exposure to neutrons. The response of these integrators, which are cadmium-covered polyethylene cylinders, 15 cm in height and diameter, is not strongly dependent on the neutron energy between 20 keV and 20 MeV. The experimentally determined calibration factor is 2970 ± 180 n-mg/cm^2 for converting foil saturation activity per mg to neutron flux.

The calibrated flux integrators were used to measure neutron fluences from the accelerators at both medical facilities. With a 20 x 20 cm field size and 100 cm target distance, the Varian Clinac 1800 fluences ranged from $(1.80\pm0.11)\times10^5$ n/cm^2-rad$_x$ (4.29±0.27 mrem$_n$/rad$_x$) at 20 cm from the beam axis to $(8.96\pm0.56)\times10^4$ n/cm^2-rad$_x$ (2.13±0.14 mrem$_n$/rad$_x$) at 100 cm from the beam axis. These were measured on the treatment table and without patients. Beside the treatment table (about

35 cm from the beam axis) the detectors averaged $(1.235\pm0.010)\times10^5$ $n/cm^2\text{-}rad_x$ (2.938 ± 0.024 $mrem_n/rad_x$). Experiments at the table side location during patient therapy were of the same order of magnitude as those done without patients, lending credibility to the technique.

For the 10 MV Saturne 1, an average fluence of $(5.985\pm0.035)\times10^4$ $n/cm^2\text{-}rad_x$ (2.497 ± 0.014 $mrem_n/rad_x$) was found at 20 cm axial distance on the table, 20 x 20 cm field size. At 100 cm axial distance with the same field size, an average fluence of $(2.720\pm0.048)\times10^4$ $n/cm^2\text{-}rad_x$ (1.134 ± 0.020 $mrem_n/rad_x$) was found. These values are somewhat greater than half the fluence from the Varian Clinac 1800 for the same conditions.

NEUTRON FLUENCE AND DOSE FROM

A VARIAN CLINAC 1800 ACCELERATOR

I Introduction

Problem

The problem addressed in this thesis study is the determination of the neutron flux and/or dose output from an electron accelerator. Specifically the goal was to measure the neutron dose a cancer patient receives while undergoing x-ray treatment with the high-energy electron accelerator at the WPAFB Medical Center.

Activation of gold foils was the method used for these neutron measurements. When gold foils are exposed to a neutron flux, such as from the electron accelerator, some of the gold atoms absorb a neutron and become radioactive. Thus it is necessary to relate the foil's activity (as measured by some specified detector system) to the neutron fluence that induced said activity.

The solution of the problem above was easily divided into four main steps. First a series of gold foils were activated in a neutron pile with a known thermal neutron flux. This activity was used to determine the efficiency of the detector used to count the foil activity. Second was a calibration of the response of the neutron flux moderators to a known neutron flux (not the thermal flux in part one above). Third, the calibrated neutron flux moderator was used to measure the unknown neutron flux from the Medical Center's accelerator. Last, a neutron fluence-to-neutron-dose conversion was applied to give the expected dose a patient would receive. These steps are explained in detail later.

Background

The WPAFB Medical Center has a high-energy electron accelerator - specifically, a Varian Clinac 1800 - which is used in radiation therapy for cancer patients. To produce x rays the electron beam is targeted onto a material which has a high atomic number, typically copper or tungsten. The Varian Clinac 1800 has a tungsten target. Rapid deceleration of the electrons in this target produces bremsstrahlung x-ray photons. These high-energy photons irradiate the cancerous tissue as part of the therapy.

To direct the x rays into a beam, a filter-collimator assembly is used to channel the x rays. These assemblies are usually of lead or tungsten. The Varian Clinac 1800 uses tungsten.

If the energy of the photons exceeds the binding energy of the neutrons in the target material then neutrons can be expelled due to photonuclear reactions. Most nuclei have binding energies between 7 and 11 MeV (NCRP 31:14). Lead and tungsten - both used in accelerator heads - have binding energies near 7 MeV (McGinley et al, 1976:397); the lead cross-section peaks at 13 MeV (NCRP 31, 1964:14). Some neutrons are also produced by electron interaction, but the probability for ejection of neutrons directly by this method is about 100 times smaller than for photons (NCRP 31, 1964:14). The WPAFB accelerator produces electron energies of either 6 or 18 MeV for x-ray treatment. Since most cancer therapy is conducted at 18 MeV, neutrons are produced. This is an undesirable, though unavoidable, side effect. These neutrons cannot be collimated as the x rays can; thus the patient receives a whole-body dose of neutrons. It is desirable to know the dose of neutrons received and to make certain that it remains a negligible part of the total dose.

To measure the neutron dose, knowledge of both the neutron flux and

the energy spectrum of the flux are needed. A detection system for measuring neutron flux in an accelerator environment must meet two conditions. First it must be insensitive to the intense photon flux present. Secondly it must be sensitive to the neutrons. Neutron detection by activation of gold and indium foils meets both conditions. Gold and indium have a low cross section for photonuclear reactions and a high cross section for neutron absorption; thus both materials will absorb neutrons while being unaffected by photons. The maximum activity that can be induced in the foil is equal to the rate of radionuclide production by neutron absorption; this maximum activity is called the saturation activity. The rate of neutron absorption is directly proportional to the flux of neutrons across the foil; the activity is proportional to the fluence (integrated flux) of neutrons over a given time. Thus the induced foil activity can be used to calculate the neutron fluence when certain conditions prevail. If the spectrum of neutrons is known, the whole-body neutron dose can be determined. Combining this fluence with estimates of neutron interaction with tissue allows determination of a whole body neutron dose.

A prior researcher at AFIT working on the problem of neutron dose from medical accelerators used Bonner spheres (polyethylene spheres of various diameters) to determine the neutron spectrum, and flux integrators (cadmium covered polyethylene cylinders, 15 cm in height and diameter) and cadmium-difference pairs to measure neutron flux (Rossano, 1989:23). Though unable to measure the neutron fluence at the base medical center, he did measurements at Miami Valley Hospital to test the neutron measurement methods developed. He reported dose rates of 1.5 millirem per rad of photons (Rossano, 1989:55).

Scope of Thesis

Part of the goal of this thesis is to verify and improve upon, if possible, the factors found earlier by Rossano to relate counts from activated gold foils to neutron fluences (which caused the activation). This requires using much of the same equipment and procedures that he used for his report. The other goal is to use the flux integrators to measure the neutron fluence at the WPAFB cancer-therapy accelerator.

To deduce the flux of neutrons that activated a particular foil the neutron spectrum must be known or certain assumptions must be made about it. In this continued work the spectrum was not to be determined. Instead the assumption was made that the photoneutron spectrum is similar to that of fission neutrons (McGinley et al, 1976:397; Nath et al, 1984:233; Rossano, 1989:18-19). The average energy of such photoneutron spectrums is around 1.0 MeV (Nath et al, 1984:233; Holt et al, 1979:428). Also the detector system used has a uniform response over the neutron spectrum present. Specifically the flux integrators "flatten out" the spectrum and so lessen the dependence of the foil activation on the spectrum present (McGinley et al, 1976:399; Bruninx, 1970:658). The spectrum determined previously by Rossano was assumed typical of what will be encountered, with an average energy of approximately 1 MeV for the neutrons from the electron accelerator (Rossano, 1989:52).

The flux integrators, gold foils and cadmium covers used in this project are the same ones used by Rossano. This equipment is described in later parts of this paper, but their usage is briefly described here.

The bare- and cadmium-covered foils were exposed to neutrons in the standard graphite pile in the basement of Building 470. Since the thermal flux in the pile is known, one can calculate the saturation activity

of these pairs. The known activity can then be used to determine the counting efficiency of the Geiger-Mueller detector system used for counting activated gold foils.

The flux integrators containing gold foils were exposed to a known neutron flux from a bare PuBe source in the dome area of Building 470. The activity of these foils, determined by the calibrated Geiger-Mueller counter, was used to obtain the calibration constant for the flux integrators.

Measurements at the hospital were made with and without patients being present. These measurements were used to calculate the fluence of neutrons under various operating conditions of the accelerator, from which a dose can be calculated if the spectrum of neutrons is known.

Outline of Thesis Document

The remainder of this report gives the theory and methods used for confirming and applying foil activation for neutron monitoring of the electron accelerator. Chapter II summarizes the theories behind foil activation for determining neutron flux, and introduces conversion factors for calculating neutron doses. Chapter III describes the equipment and experimental methods used. Chapter IV gives the results of the neutron measurements. Chapter V sums up the conclusions from the results, along with suggestions for further investigation. A series of appendices follow.

Uncertainties in data values were determined by propagation of error (Bevington, 1964:56-64) except where otherwise noted. A different method was used only in one circumstance, where the application of prop-

agation of error produced unreasonable results in the uncertainties. In that instance a statistical formula was used (Bevington, 1964:93). All uncertainties are given at the one sigma level.

II Theory

Neutron Activation Method

For this report, neutron fluxes and fluences are measured by foil activation. This technique is useful for a variety of situations in which other methods are impractical. For instance, the environment to be measured may be hazardous to humans for the time of measurement, or it may contain other types of radiation that would flood a real-time detector. An electron accelerator falls in the latter category.

Gold has excellent properties for detecting thermal neutrons by activation. It has a single stable isotope, ^{197}Au, that has a large absorption cross section of 97 barns for thermal neutrons and a low cross section for photonuclear reactions. The activation product, ^{198}Au, decays with a half life of 2.6935 days. In 99.975% of its decays, ^{198}Au decays by beta emission to an excited state of mercury (NCRP 58, 1985:489). In about 95% of the decays the excited mercury atom emits a 411-keV gamma ray; in about 5% an internal conversion electron of about 340 keV is produced. These modes of decay make it relatively simple to measure activation by measuring either beta or gamma decay.

Whatever material is used in neutron activation, the theory is the same. The reaction rate R for neutron interactions in a volume V is given by the neutron flux ϕ times the total activation cross section Σ_{act}, or

$$R = \phi \Sigma_{act} V \qquad (1)$$

(Knoll, 1979:766). The activation cross section in this equation is the

average cross section for the entire neutron spectrum since σ depends on the neutron energy. One can also express this as $\Sigma = N\sigma$ where N is the total number of target atoms per volume in the material being activated and σ is the flux-averaged microscopic cross section. Given the cross section and fluxes are energy dependent terms then we must express the reaction rate as an integral over energy,

$$R = N_T \int_0^{\infty} \sigma(E)\phi(E)dE \tag{2}$$

(Price, 1964:314) where N_T represents the total number of atoms in the target material.

The microscopic neutron cross section for gold has a 1/v (where v is velocity) dependence for thermal neutrons, that is, neutrons less than about 0.5 eV. Thus $\sigma v = K$ where K is a constant. It is advantageous then to choose some reference cross section and velocity σ_0, v_0, and express the cross section in terms of these. The 0 subscript indicates the most probable value for a Maxwellian distribution. When the integral for reaction rate is divided into a thermal and epithermal region, the reaction rate term in the thermal region becomes

$$\begin{aligned} R_{th} &= N_T \int_0^{0.5} \frac{\sigma_0 v_0}{v}\phi(E)dE \qquad (3) \\ &= N_T \int_0^{0.5} \frac{\sigma_0 v_0}{v} n(E) v dE \\ &= N_T \sigma_0 v_0 \int_0^{0.5} n(E)dE \\ &= N_T \sigma_0 v_0 n_{th} \end{aligned}$$

where n_{th}, the number of neutrons per unit volume with energies less than or equal to 0.5 eV, is called the thermal neutron density.

Now the material being irradiated with neutrons also undergoes radioactive decay as the radioactive atoms are formed. The time rate of change of radioactive atoms is simply the rate of activation minus the rate of decay, or

$$\frac{dN}{dt} = R - \lambda N \tag{4}$$

where N is the number of radioactive atoms and λ is their decay constant. Assuming N=0 at time t=0 the solution to this equation is

$$N(t) = \frac{R}{\lambda}(1 - e^{-\lambda t}) \tag{5}$$

The activity A(t) is then

$$A(t) = \lambda N(t) = R(1 - e^{-\lambda t}) \tag{6}$$

After a very long time - say, 10 half-lives or more - we have $A_\infty = R$ for the saturation activity. This value will be used later in calculating the neutron flux. It is impractical to irradiate the material to its saturation activity, but this value can easily be calculated. If the time of exposure t_e, the time between end of irradiation and beginning of counting t_w, and the time of counting in the detector t_c along with the net counts (total counts minus background) are known then the saturation activity may be calculated according to the relation,

$$A_\infty = \frac{\lambda C_{net} e^{\lambda t_w}}{\epsilon(1 - e^{-\lambda t_e})(1 - e^{-\lambda t_c})} \tag{7}$$

(Knoll, 1979:767) where ϵ is the counting efficiency of the detector.

Cadmium Difference Theory

The saturation activity can be divided into the activity contributed by the thermal neutrons and that contributed by the epithermal neutrons,

$$A_\infty = A_{\infty(th)} + A_{\infty(e)} = N_T \sigma_0 v_0 n_{th} + A_{\infty(e)} \tag{8}$$

A cadmium cover of about 0.02 inches thickness serves to block thermal neutrons while allowing epithermal and fast neutrons to irradiate gold foils within the cover. By irradiating gold foils with and without cadmium covers one can measure the difference in activity induced by only epithermal neutrons and activity induced by all neutrons. This difference represents the thermal neutron contribution. In practice a correction factor F_{Cd} must be applied to the epithermally induced activity since the cadmium does absorb some of the epithermal neutrons. This correction factor is dependent upon the thickness of the cadmium cover, and to a lesser extent on the thickness of the gold foil (Price, 1964:337). Values reported in the literature range from 1.013 to 1.04 for cadmium covers 20 to 40 mil thick over gold foils up to about 4 mil thick (Price, 1964:337; Martin, 1955:53; WADD, 1960:21). Previous researchers have used F_{Cd}=1.04 when working with the AFIT neutron pile (Rossano, 1989:63; WADD, 1960:21) and cadmium covers of nominally 30 mil

(Rossano, 1989:63). Thus by replacing and rearranging in the above expression the induced thermal neutron activity may be written according to

$$N_T \sigma_0 v_0 n_{th} = A_\infty - F_{Cd} A_\infty(Cd) \tag{9}$$

where $A_\infty(Cd)$ is the saturation activity induced in the cadmium covered foil. At this point a correction F_{th} may also be made because of the neutron flux depression due to absorption by the foil. However, the contribution by thermal neutrons to the activity of 20-mil cadmium-covered gold foils is less than 0.1% of the total activity (WADD, 1960:21). This uncertainty is negligible in comparison to other uncertainties in this experiment, so it may be neglected.

From Eq. (9) the thermal neutron density may be written as

$$n_{th} = \frac{A_\infty - F_{Cd} A_\infty(Cd)}{N_T \sigma_0 v_0} \tag{10}$$

Now the total thermal flux is given by $\phi_{th} = n_{th} v_{av}$. Since the average velocity in a Maxwell-Boltzmann distribution is 1.128 times the mc-t probable velocity (i.e. $v_{av} = 1.128 v_0$), the previous equation may be rearranged to give (with F_{th} now included for completeness)

$$\phi_{th} = 1.128 F_{th} \frac{A_\infty - F_{Cd} A_\infty(Cd)}{N_T \sigma_0} \tag{11}$$

Using activity per unit mass is a bit more convenient than entering

the total number of atoms in each foil. The total number N_T may be expressed in terms of mass by

$$N_T = \frac{Mass N_a}{AW} \tag{12}$$

where N_a is Avogadro's number, AW is the atomic weight of gold and Mass is the weight of the gold foil. This substitution into (11) gives

$$\phi_{th} = 1.128 AW \frac{A_\infty - F_{Cd} A_\infty(Cd)}{\sigma_0 N_a Mass} \tag{13}$$

By introducing a specific activity, S_∞ such that

$$S_\infty = \frac{A_\infty}{Mass} \tag{14}$$

Equation (13) may be rewritten as

$$\phi_{th} = 1.128 AW \frac{S_\infty - F_{Cd} S_\infty(Cd)}{\sigma_0 N_a} \tag{15}$$

This is the equation used in this study for the standard pile foils. The known ϕ_{th} for the pile is used to calculate S_∞ for use in the calibration of the Geiger-Mueller counter.

Neutron Moderators and Thermal Neutron Measurements

Neutrons emitted by a neutron source are often divided into two or three groups, depending upon their energy. Less energetic neutrons are usually designated as thermal neutrons. More energetic neutrons are designated as epithermal or as fast. The dividing point between thermal and epithermal is generally taken at about 0.5 eV; at this energy the absorption cross section for cadmium, which is often used to block thermal neutrons, has a very steep drop.

Gold is useful as a thermal neutron detector because of its high cross section for thermal neutron capture (approximately 97 barns). In a fast neutron environment, the neutrons must be slowed down if the detector depends on thermal neutron capture cross sections. To slow down (or moderate) the neutrons, a material is needed whose atoms are approximately the same mass as the neutron. If the scattering particles are of a different mass than the neutron, near-inelastic scatters occur whereby the neutrons retain their high energies. Most organic materials are adequate moderators since hydrogen makes up a large portion of their atomic composition. Polyethylene is often used as a neutron moderator; indeed, the flux integrators used for this project have a cadmium cover over a polyethylene interior. The cadmium blocks thermal neutrons so essentially only fast neutrons enter. Once in the polyethylene, the neutrons collide with hydrogen atoms. Energy exchange to the hydrogen slows the fast neutrons to thermal energies. The resulting thermal neutrons are isotropic in direction, due to scatter after giving up energy in interaction with hydrogen atoms. A gold foil within the polyethylene is thus subject to a flux of thermal neutrons, and will absorb them according to its cross section for thermal neutron capture. A given flux will then result in radioactive gold atoms.

Gold also has a resonance cross section varying from about 1-50 barns for neutrons of about 0.1-1 keV, and a narrow peak of several thousand barns at 5 eV (Garber and Kinsey, 1976:400). Since the flux integrators thermalize the neutrons to energies less than 1 eV (which is below the resonance interval) and since the resonance cross section is smaller than the thermal cross section, the resonance cross section was not considered important in this study.

The procedure may be summarized according to the following description. The flux integrators are calibrated by exposing them to a known neutron flux, with gold foils inserted in the flux integrator. This will show how the flux integrators respond to neutrons with a known flux and spectrum. Then the assumption is made that the neutron spectrum from the neutron source and from the electron accelerator are close enough to give the same response in the flux integrators: i.e. the response of the flux integrators is not strongly dependent on the neutron spectrum. This is reasonable given the spectrum-flattening characteristics of the flux integrators. Their energy response varies little in the 20 keV to 20 MeV range (Reactor Experiments, Inc., undated:1; McGinley et al, 1976:399; Sanders et al, 1984:107). Once calibrated, the flux integrators are exposed to the neutron environment around the accelerator. From the foil count rates, combined with the counting efficiency of the Geiger-Mueller detector and the calibration factor for the flux integrators, the neutron flux from the accelerator can be deduced.

Neutron Dosimetry

The important radiation considerations from neutrons result not from primary interaction of neutrons with tissue, but from secondary

radiation caused by the neutrons. Thermal neutrons - that is, those below about 0.5 eV - interact chiefly through neutron capture by atoms within the body. These interactions are capture by nitrogen, $^{14}N(n,p)^{14}C$, and capture by hydrogen, $^{1}H(n,\gamma)^{2}H$. From just above thermal energy to about 10^{-4} MeV, (n,p) reactions are the dominant energy transfer mechanism. Above this, most of the energy and dose deposition is by elastic scattering of hydrogen nuclei (Attix, 1969:468).

NCRP presently recommends a quality factor (QF) of 20 for converting absorbed neutron dose (measured in rads or centigrays) to equivalent dose (measured in rems or centisieverts). Quality factors are used to indicate the expected biological effect of a unit of radiation; different types of radiation will affect tissue differently (based on the linear energy transfer (LET) of ionizing radiation in tissue). Alternately if a factor for converting neutron fluence to equivalent dose is known, the neutron dose can be calculated by simply applying this conversion factor to the measured fluence. This alternate procedure was used in this study.

Neutron Dose Conversion

A number of studies have been done which relate neutron fluence to photon dose, neutron dose to photon dose, and neutron fluence to neutron dose. These relations are usually based on the average energy of the neutron spectrum, which in turn depends on the photon energy and the target, flattener, and collimator assembly materials. For comparison and reference a table of conversion factors from the literature is given in Appendix A, sorted by units.

The Varian Clinac 1800 runs at 18 MeV. Hence it is reasonable to expect between 7.2×10^4 n/cm^2-rad$_x$ and 1.7×10^5 n/cm^2-rad$_x$, based on the last two entries of part b. of the table in Appendix A.

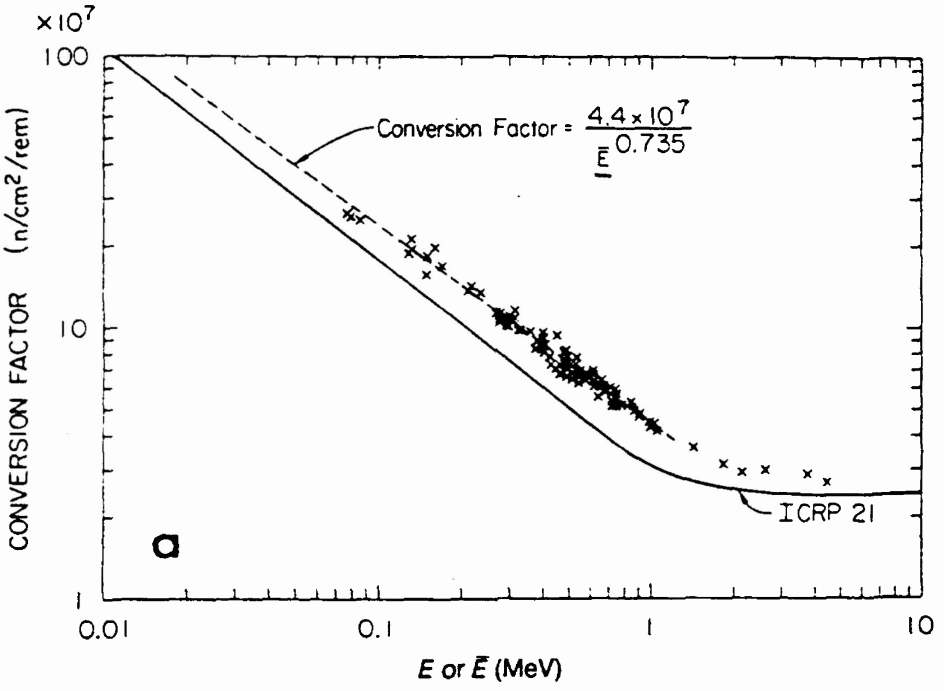

Figure 1 Dose Equivalent to Neutron Fluence

Figure 1 is a graph of the relation between neutron fluence and neutron dose equivalent, based upon the energy of the neutrons (or the average energy for a spectrum). Using an average neutron energy of approximately 1 MeV for tungsten photoneutrons (Toms and Stephens, 1957:77-81) a conversion factor of 2.38×10^{-8} rem$_n$-n/cm^2 was used for neutron flux to dose calculations for the Varian Clinac 1800 (McCall and Swanson, 1979:77). If the predominate material in the accelerator head were lead (as with the CGM Saturne 1 accelerator at Kettering), the average photoneutron energy would be about 2 MeV (NCRP 79, 1979:30) and

a factor of 4.17×10^{-8} rem_n-n/cm^2 would be appropriate for the neutron flux to neutron dose conversion factor. (NCRP 79, 1979:45; McCall and Swanson, 1979:77). Note these two conversion factors are the inverse of the factors in part d. of the table in Appendix A. Indeed, part d. was derived from Figure 1. These factors are already given in rems, so they were used here as given. Note, however, that a set of quality factors was used in converting D(rads) to H(rems). Recent recommendations by the ICRP and NCRP are to double previous quality factors. If adopted, all the doses above should be doubled.

Once the neutron fluence is known, then, the neutron dose can be calculated by the formula

$$H = \left(2.38 \times 10^{-8} rem_{n_0}^{1} n/cm^2\right)\Phi \qquad (16)$$

for the neutrons from the WPAFB electron accelerator (which uses tungsten). For measurements done on the Kettering CGM Saturne 1 (which uses lead), the conversion from fluence to equivalent dose is given by

$$H = \left(4.17 \times 10^{-8} rem_{n_0}^{1} n/cm^2\right)\Phi \qquad (17)$$

III Method and Apparati

Equipment

The equipment used for this study include the gold foils and cadmium covers, the flux integrators, a Geiger-Mueller detector system, radioactive sources, and the AFIT standard graphite pile. All this equipment was already on hand at AFIT before this project was begun.

Eighty-four gold foils were used. The supplier assayed them as 99.99% pure. The diameter and thickness of the foils are nominally 1 inch and 0.001 inch respectively. Their masses range from 242.9 to 300.7 mg. Their thicknesses range from 47.4 to 59.0 mg/cm^2. (Specific parameters of each foil are given in Appendix B.) Tweezers were used to handle them so there would be no contamination from handling.

The cadmium covers are 1 inch in diameter, just large enough to hold the gold foils. They varied in thickness from 0.027 to 0.033 in. This thickness is sufficient to block out thermal neutrons, but allows most of the epithermal (fast or resonant) neutrons through to irradiate the gold foils within the cadmium covers. The effect on F_{Cd} from the variation in cadmium thickness was considered to be less than other uncertainties and therefore neglected. Previous work with the graphite pile used this same F_{Cd} (Rossano, 1989:63; WADD, 1961:21), and these were the same covers used by Rossano in the previous study.

The G-M detection system was assembled from several separate pieces of equipment. At its core is a thin window, pancake style G-M tube, Model N1002 made by TGM Detectors. It is filled with neon and quenched with a halogen fill gas. The window is mica with a graphite coating.

The diameter is 44 mm and the thickness is about 2.0 mg/cm^2. The mounting tray is stainless steel. The detector and tray are set in a "box" comprised of lead bricks to shield it from extraneous radiation. A silver backscatterer was always used with this assembly.

The AFIT standard graphite pile consists of 18 crossed layers of 4" x 4" x 50" reactor-grade graphite. The pile is encased in 1/32" cadmium to prevent the escape or entry of thermal neutrons. The pile has 9 sliding elements in which the gold foils can be placed for irradiation.

The neutron source for the graphite pile, M580, is a Pu-Be source. Its output was 1.06×10^7 neutrons/second in September, 1989. (The correction to the output is shown in Appendix C. Its output as specified by the manufacturer was 8.86×10^6 neutrons/second in June, 1960 (Mound, 1960:1)). This source was used for all the foil irradiations in the graphite pile.

The neutron source used in the reactor dome, M1170, is also a Pu-Be source with output of 1.1×10^7 neutrons/second on 23 June, 1989 (calculation for this activity is in Appendix C). Its output as specified by the manufacturer was 9.00×10^6 neutrons/second on 2 March, 1962 (Mound, 1962:1).

The flux integrators are illustrated in Figure 2. They are cylinders with a diameter of 150 mm and a height of 150 mm. They are made of high density (0.95 g/cm^3) polyethylene with a 0.50-mm thick cadmium cover to block thermal neutrons from entering and prevent thermalized neutrons within from escaping. A well of 5-cm diameter and 7.5-cm depth was drilled into the flux integrators. A matching polyethylene plug with a cadmium disk at one end was made to fill the well (Rossano, 1989:25). The foils are inserted into the bottom of this well for irradiations.

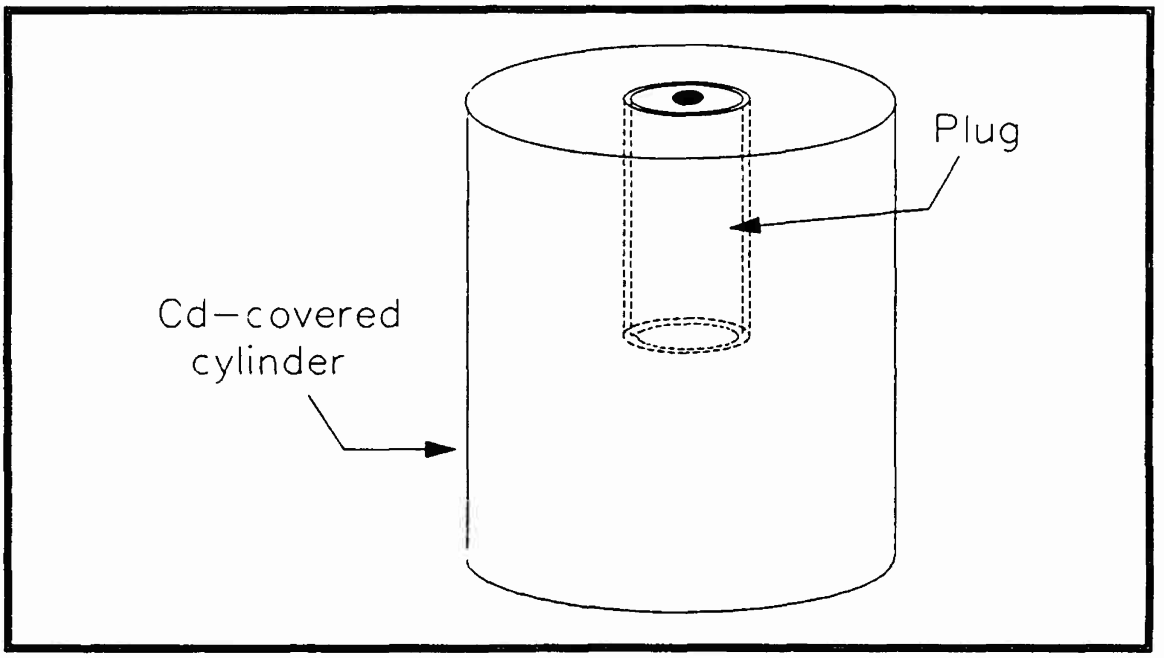

Figure 2 Flux Integrator

Neutron Pile Measurements

The standard graphite pile at AFIT was used to calibrate the efficency of the beta counting detectors. The graphite pile consists of 18 criss-crossed layers of reactor grade (AGOT) beams. Each beam measures 4"x4"x50" and each layer is 4" thick, 48" wide, and 50" long. The resulting assembly is covered on all sides by a 1/32 inch (0.8 mm) layer of cadmium. This prevents thermal neutrons from escaping the pile and also prevents thermal neutrons from entering the pile. The cadmium layer is further enclosed by an aluminum honey-combed insulating panel.

Several beams in the pile are fashioned to be easily pulled in and out of the pile. These beams are known as stringers. The neutron source, M580, fits into a recess in the source stringer, in the fourth layer from the bottom of the pile. Nine foil stringers , FS-1 through

FS-9, are located in every odd layer beginning from the bottom layer of the pile. These stringers have holes drilled into them to hold foils; graphite plugs are also inserted with the foils to space foils appropriately and to surround the foils with graphite rather than an empty space.

Thermal neutron flux in the graphite pile is measured by the cadmium difference method. Bare foils are irradiated in the foil stringers, and then cadmium-covered foils are irradiated in the same location. The cadmium cover blocks thermal neutrons so that only fast neutrons activate the foils. The difference in the activity of the bare and cadmium-covered foils is attributed to thermal neutrons, as was described in Chapter II.

Hospital Measurements

The flux integrators were used at the x-ray cancer therapy machine at both the Wright Patterson Medical Center and at Kettering Memorial Hospital. Measurements were made both with and without patients present. Descriptions are given in the following sections.

Measurements Without Patients

A series of gold foil irradiations in the flux integrators was made in the accelerator room with no patients present. For the first set of measurements, the top of the treatment table was set at 107.5 cm below the target of the machine. This puts the plane of the gold foils at 100 cm from the target, since the flux integrators are 15 cm in height and the foils are located at the midpoint of the integrator. The flux integrators were placed along the mid-line of the table, at distances of 20 cm, 30 cm, 50 cm, and 100 cm from the beam axis. These were done two

at a time, with the flux integrators being set on opposite sides of the beam axis; for instance, one flux integrator might be set with its center 20 cm from the beam axis towards the head of the table, and another set with its center 100 cm from the beam axis, but towards the foot of the table. This prevented one flux integrator from being in the way of the other flux integrator as seen from the beam axis.

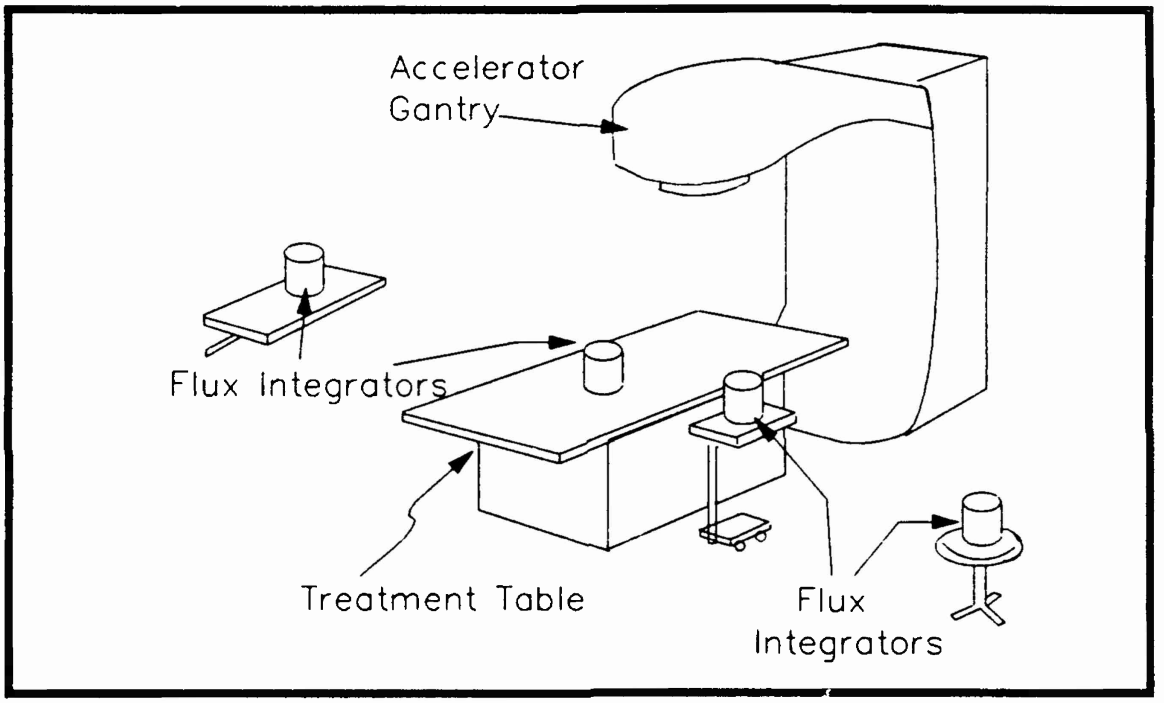

Figure 3 Accelerator Room Composite Setup

Another set of neutron measurements were taken at four positions off of the table, perpendicular to both the beam axis and the table length. One position was on a medical stand abutting the table and at the same height. This was the same placement used for measurements

during patient therapy. Two measurement positions were on chairs 2 meters on either side of the table. These were not at the same height as the table, nor were they at identical heights. Another position was with a flux integrator set on a chair 4 meters to one side of the table. Figure 3 gives relative locations of the positions.

Table 1: Flux Integrator Locations in Accelerator Room

Position Relative to Vertical Mid-Plane of Table	Height of Plane of Bottom of Flux Integrator	Straight Line Distance from Target
Next to table (on medical stand)	107.5 cm below plane of target	106.5 cm
2 meters (towards far wall of room)	84.5 cm above floor (set on table)	232.7 cm
2 meters (towards entrance of room)	63.5 cm above floor (set on a stool)	244.13 cm
4 meters (towards entrance of room)	63.5 cm above floor (set on a stool)	423.79 cm

The straight line distances from the target head to these foil positions were calculated geometrically. The target head is 203.5 ± 0.5 cm above the floor of the treatment room. The foil heights are given in Table 1. The difference in foil height and target height defined one side of a triangle for each position; the distance from the center of the table to the foil positions defined the base of such triangles. The hypotenuses of these triangles gave the straight-line distances, as recorded in Table 1. At the "next to table" position the flux integrators were taken as being centered 36.6 cm from the beam axis (55.3 (table width) + 2 + 7.5 (flux integrator radius) + 1.5 (estimated distance from edge of table to edge of flux integrator, due to edge on

medical stand which prevented flux integrator from directly abutting the table)). The straight line distances for all the measurements in Table 1 refer to the distance from the center of the flux integrators (where the foils are situated) to the center of the target head, and may be taken as valid within 2 cm.

Measurements With Patients

A series of flux integrator measurements were made during cancer therapy with patients present. All measurements were made for treatments with 18 MV x rays. The accelerator is normally set at 240 monitor units/minute. The accelerator is calibrated to deliver 1 rad per monitor unit at depth of maximum dose in water (which corresponds approximately to tissue, since human tissue is > 80% water). This depth is 3.2 cm for 18 MV x rays.

For patient treatments, it was of course impossible to set the flux integrators on the table as was done for non-patient irradiations with the accelerator. Instead the flux integrators were set on a medical stand set at the same height as the table. This stand was set as close as possible to the patient and table, next to the area being irradiated. Here it was hoped to capture the maximum dose of neutrons near the patient. (At this position the center of the flux integrator is 36.6 ± 2.0 cm from the beam axis, as calculated in the previous section.)

IV Experimental Results

Thickness Dependencies of Gold Foil Counting

The thickness of a foil affects the activation of the foil through self-shielding and self-absorption. It was important to account for these processes because the foils used in this procedure were not infinitessimally thin, nor were they of exactly uniform thickness. The majority of foil activation was done with one mil foils, i.e. 49 mg/cm^2. However, these foils are only nominally one mil since they varied in thickness from about 45 mg/cm^2 to about 55 mg/cm^2.

Self-shielding occurs during foil activation. Gold atoms on the outside of the foil block some neutrons from entering the foil. This shields atoms deeper within the foil from neutrons that might activate them. Self-absorption occurs during counting of the activated foil. Beta and gamma radiation emitted from atoms within the foil must travel through several layers of atoms to reach the surface. Atoms nearer the foil surface act to absorb this outgoing radiation; hence the term self-absorption. Beta radiation is absorbed to a greater extent than is gamma radiation. Since the detection system used was a beta counting system, self-absorption is an important factor.

It is rather difficult to separate self-shielding and self-absorption. Experimenters have traditionally combined these two processes into a single correction factor. The same was done here.

To develop this factor, four half-inch foils, of 0.5-mil nominal thickness, were used in the standard graphite pile. Four such foils will fit into the same stringer location in the pile without overlapping each other. There they experience the same neutron flux and the same

activation. These foils were then counted in the G-M detector. They were counted separately, then in stacks of two, three and then all four together. The saturation count rate (units of s^{-1}) was computed by

$$C_s = \frac{\lambda C_{net} e^{\lambda t_w}}{(1 - e^{-\lambda t_c})(1 - e^{-\lambda t_e})} \tag{18}$$

(from Eq (7), $A_s = C_s/\epsilon$). An expression for the thickness factor was obtained from a linear regression plot of the saturation count rate per thickness, C_s/x (where x is thickness in mg/cm^2) versus the thickness in mg/cm^2 on a semi-log plot. Another expression for the thickness factor was obtained by plotting the saturation count rate per mass, C_s/mass (where mass is given in mg) versus the thickness. These plots are shown in Figures 4 and 5. The data for these plots are in Appendix D. The relation for C_s/x vs x was found to be

$$\frac{C_s}{x} = (2.606 \pm 0.036)\exp[(-0.01046 \pm 0.00031)x] \tag{19}$$

and the relation for C_s/mass vs x was found to be

$$\frac{C_s}{mass} = (1.984 \pm 0.026)\exp[(-0.01044 \pm 0.00031)x] \tag{20}$$

The exponential portions of these terms are not statistically different from the value found by a prior researcher. The value found previously is μ = -0.0104 ± 0.0011 (Rossano, 1989:35).

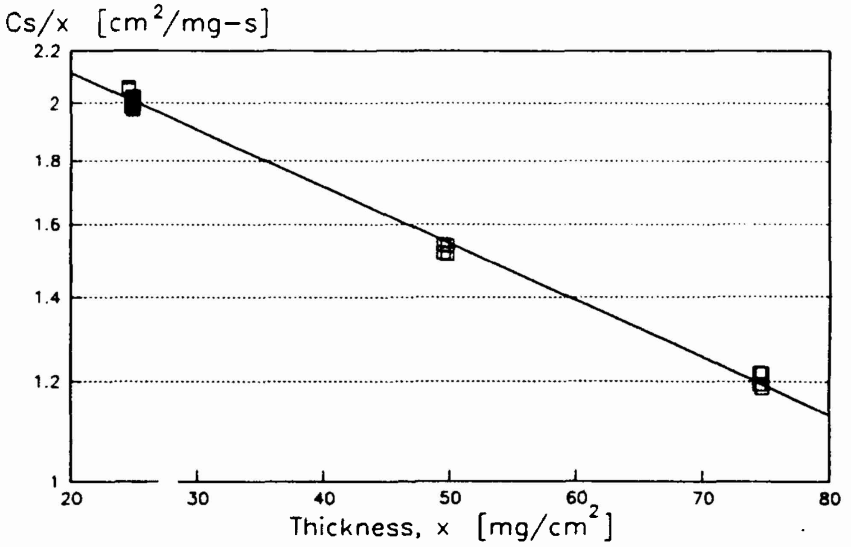

Figure 4 Saturation Counts/Thickness vs Thickness

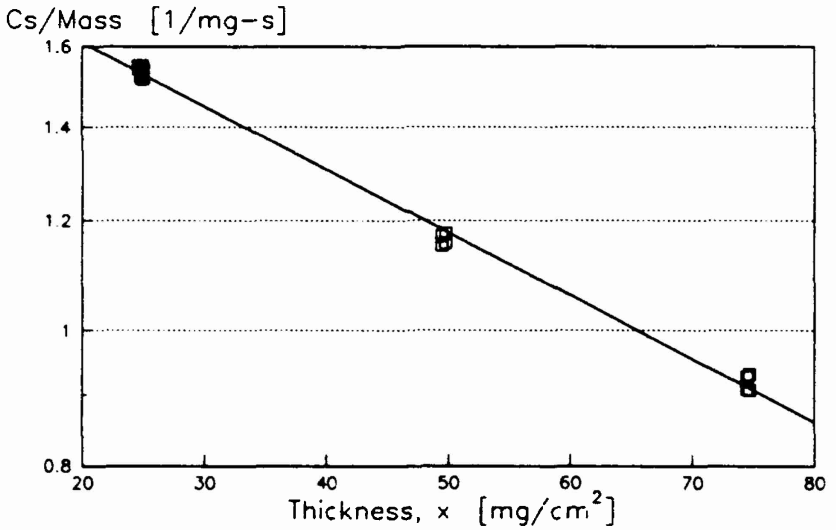

Figure 5 Saturation Counts/Mass vs Thickness

Detector Efficiency Determination

The gold foil irradiations in the graphite pile were used to determine the counting efficiency of the beta counting systems used. The detector system used was a Geiger-Mueller detector with a silver backscatterer in the counting chamber. Two sets of cadmium difference pairs of gold foils were irradiated in stringers 1 through 6 of the pile. First foils were irradiated bare (without cadmium covers) and counted in each detector system to get total activity. Then a similar set was irradiated in the cadmium covers and counted. The resulting data gives comparisons between detector systems and with previous results by Rossano.

The thermal neutron flux at each stringer location is well known, and thus may be used in the flux equation to finalize the counting efficiency term, ϵ, and any other constant terms necessary for the flux equation developed earlier. Thickness dependent terms were found above. By comparing the difference in the bare and cadmium covered foils in each stringer location and entering all other known terms into the flux equation, the only unknowns left are the constant terms in the counting efficiency term. A solution for these constants in terms of one combined constant gives a gross correction term to take care of any unforeseen terms that belong to make the flux equation work.

The constant terms before the exponentials in Eqs (19) and (20) are constants whose value depends upon what the foil thickness is compared against. The exponential portion represents the product of all the exponential terms in the efficiency, ϵ. Thus the efficiency can be written as

$$\epsilon = f_x \exp(-0.01045x) \qquad (21)$$

where f_x is a constant factor and the two exponential values above have been averaged.

The equation for ϕ_{th} in the graphite pile, using cadmium difference pairs, is given by

$$\phi_{th} = \frac{1.128\,AW}{\sigma_0 N_a} 1000 \left[\frac{C_s(b)}{\epsilon_b M_b} - \frac{F_{Cd} C_s(Cd)}{\epsilon_{Cd} M_{Cd}} \right] \tag{22}$$

where the subscripts b and Cd refer to bare and cadmium covered foils respectively. The factor of 1000 is the conversion from milligrams to grams, since masses were measured in milligrams and AW is taken as grams/mole. If a variable $\epsilon' = \exp[(-0.01045)x]$ is introduced then from the previous paragraph $\epsilon = f_x \epsilon'$. The equation for ϕ_{th} can be written

$$\phi_{th} = \frac{1.128\,AW}{\sigma_0 N_a} \frac{1000}{f_x} \left[\frac{C_s(b)}{\epsilon_b M_b} - \frac{F_{Cd} C_s(Cd)}{\epsilon_{Cd} M_{Cd}} \right] \tag{23}$$

In the graphite pile ϕ_{th} is known for each location. All other terms can be determined leaving f_x as the only unknown. So $\phi_{th} f_x$ can be found for cadmium difference pairs in each stringer location in the pile. Dividing $\phi_{th} f_x$ by the known ϕ_{th} gives f_x for each case. Two such measurements were done in each of stringer locations 1 through 6 in the AFIT graphite pile. A linear least squares fit was done of ϕ vs ϕf_x. The graph of this fit is given in Figure 6; the data are in Appendix E. The value of f_x from this fit was taken as f_x for all further calculations involving efficiency ϵ. By including this f_x it was found that

$$\epsilon = (0.428 \pm 0.021)\exp[(-0.01045 \pm 0.00031)x] \tag{24}$$

where x has units of mg/cm^2. For the same detector, Rossano found (Rossano, 1989:36)

$$\epsilon = 0.431 \exp(-0.0104x) \tag{25}$$

These two efficiency terms are in good agreement.

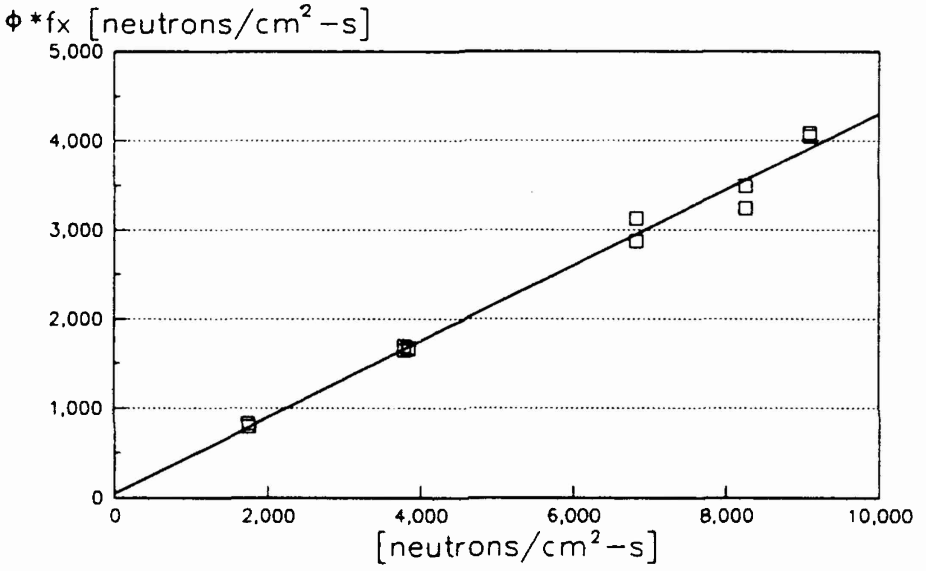

Figure 6 Finding f_x in Efficiency, ϵ

Increase of Graphite Pile Neutron Output

Calculation of the ingrowth of Am-241 in source M580 indicates the neutron output should be 19.3% higher now than the flux recorded in WADD-TR-61-174, AF NETF Graphite Standard Pile. The Am-241 ingrowth was

calculated according to a formula in this reference, and is repeated in Appendix C.

The neutron fluxes for each stringer location are given in Table 2, and reflect the increased flux since the time of the original graphite pile measurements. The original flux in 1962, as given in the WADD report, is given, followed by the expected increase flux for autumn 1989 due to the ingrowth of ^{241}Am in source M580. Then the measured flux at each stringer location, based on several measurements, is given. The nearer the ratio of the measured to calculated increase is to unity, the greater our confidence in the formulas used for calculating neutron flux. The data used for the values in Table 2 are given in Appendix E.

Table 2: Neutron Fluxes [n/cm^2-s] in Graphite Pile

Stringer	1962 Flux	Increase from Am-241	Measured Flux, Detector #3	Ratio, #3/Incr
1	3230	3853	3885 ± 148	1.008
2	6920	8256	7860 ± 287	0.952
3	7920	9449	9500 ± 343	1.005
4	5720	6824	7005 ± 251	1.027
5	3180	3794	3905 ± 141	1.029
6	1470	1754	1890 ± 71	1.078

To ensure the accuracy of the values in the table above, the present day output of M580 was compared to that of M1170 in Appendix G. The original composition of M1170 is well known from the shipping data. The original composition of M580 is less well known since no similar shipping data could be found for it at the AFIT labs. The likely fraction of ^{241}Pu in M580 was derived in Appendix C; the value found is 0.0044. If the correct fractions are used for both sources, then the

ratio of M1170 to M580 output as calculated for a particular date should agree with the ratio of measured output for that date. This was shown to be true in Appendix G.

Flux Integrator Calibration

The flux integrators were calibrated using neutron source M1170. Its output during the time of experimentation was calculated as 1.1×10^7 neutrons per second, as in Appendix C. The source and one or two flux integrators at a time were hung together at various distances (most at one meter) from each other and at heights of 25, 100, 200 and 600 cm above the concrete platform in the reactor dome of Building 470, using the assembly shown in the Figure 7.

The neutron flux at the foil location was computed by a $1/4\pi r^2$ relation. The anisotropy of M1170 (1.15 at 90 degrees orientation (Rossano, 1989:69)) and scatter from the concrete platform were also accounted for. To account for scatter from the platform the following equation was used:

$$\frac{\phi_{scattered}}{\phi_{direct}} = \frac{1.52\left(\frac{r_i}{r_0}\right)}{(1+0.1E)\left(1+\left(\frac{r_i}{r_0}\right)^3\right)} \qquad (26)$$

where r_0 is the straight line distance from source to detector and r_i is the distance traveled by a neutron which undergoes specular reflection from the source to the detector (Jenkins, 1980:44). Specular reflection simply means the angle of incidence and angle of reflection are equal.

E is the average neutron energy, in MeV, of the spectrum. For a PuBe neutron source, the average energy of the neutron spectrum is E = 4.2 MeV (Jenkins, 1980:44).

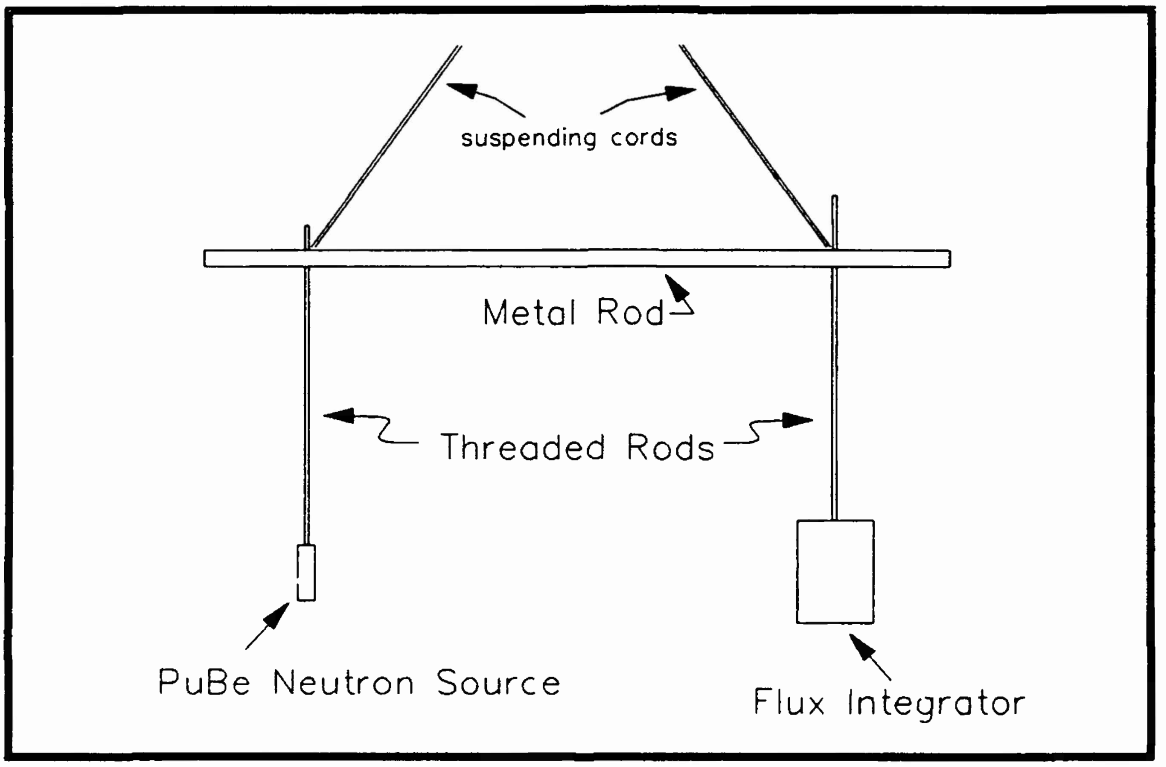

Figure 7 Assembly for Source and Detector in Dome

Since the neutron flux was known, and the saturation activity A_∞ or the saturation specific activity S_∞ was easily computed using the counting efficiency term found from the standard pile data, all that remained to be done for this part was a linear regression of neutron flux, ϕ, versus S_∞. Such an equation can be expressed by

$$\phi = K S_\infty + I \qquad (27)$$

where K represents the slope and I is the intercept. The slope of this line, which is the calibration constant for the flux integrators, was computed by linear least squares (Bevington, 1969:92; Burden and Faires, 1985:362-369). The linear regression and uncertainties were calculated using irradiation count numbers 302-306 and 332-335. (The data for these calculations are in Appendix H.) The resulting equation for the flux, given foil specific saturation activity S_a, was found to be

$$\phi = (2970 \pm 170) S_a - (7.3 \pm 6.6) \qquad (28)$$

where ϕ has units of [neutrons/second-cm^2], S_a has units of [s^{-1}mg^{-1}], and the constant K has units of [neutrons-mg/cm^2]. (Recall from Eq (14) that $S_a = A_a/Mass$). Note the uncertainty for the intercept is approximately equal to the value for the intercept. It is within the statistical uncertainty of this value to allow it to equal zero. It also makes some intuitive sense here, since if no activity is induced then one might expect there was no flux. The result above is identical with previous results, though with larger uncertainties (Rossano, 1989:38).

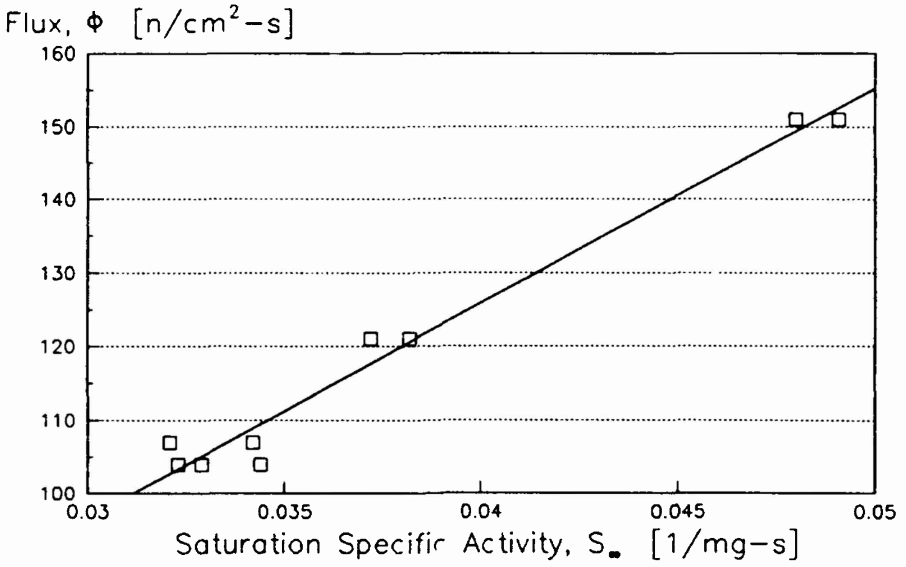

Figure 8 Least Squares Fit to Find K(E) for the Flux Integrators

WPAFB Varian Clinac 1800 Measurements

This section gives results of a series of measurements done at the WPAFB accelerator. First the measurements without patients are presented. They included measurements on the treatment table and off the treatment table; the setup for such measurements was described in Chapter III. Following these are measurements done during patient therapy.

Tables 3 through 6 give results of a series of measurements done without patients at the WPAFB Medical Center. The Field Size column refers to the size of the rectangular collimator opening in the accelerator head. Location refers to distance from the beam axis. The distance from the target to the table was 107.5 cm (so that the distance from the target to the foil in the center of the flux integrator was 100

cm). The flux was computed by the formula $\phi = KS_{\bullet}$, where K = 2970 $mg\text{-}{}^{1}_{0}n/cm^2$ from Eq. (26), and $S_{\bullet}$ is the saturation specific activity [$s^{-1}mg^{-1}$] of the gold foil. The fluence is simply the flux multiplied by the exposure time. The dose was computed using a conversion factor of 2.38×10^{-8} $rem_n\text{-}cm^2$/neutron, as suggested at the end of Chapter II for a tungsten target. The measurements at 200 monitor units (M.U.) were run at a nominal x-ray machine setting of 240 M.U. per minute. The remaining measurements, with M.U. readings of 955 to 959, were on foils exposed for 3 minutes at a nominal x-ray machine setting of 320 monitor units (M.U.) per minute. The final readings from the accelerator control board are included. Since the accelerator is calibrated so one monitor unit equals one rad_x at depth of maximum exposure in water, the relation between mrem neutron dose and x-ray absorbed dose was calculated simply by dividing the dose in $mrem_n$ by the M.U. reading.

Table 3 gives measurements done on the treatment table with the flux integrators centered 20 cm from the beam axis. Field sizes varied from 10x10 cm to 20x20 cm. The trend seemed to show a larger fluence/rad_x or $mrem_n/rad_x$ with a larger field size, but statistically there was no difference given only these data points. The two measurements with a 10x10 cm field size averaged $(1.680 \pm 0.050) \times 10^5$ $n/cm^2\text{-}rad_x$; the two measurements with a 20x20 cm field size averaged $(1.800 \pm 0.078) \times 10^5$ $n/cm^2\text{-}rad_x$.

Table 4 is the same as the Table 3, except the flux integrators were centered 30 cm from the beam axis, on the table. Again, the trend is for a larger fluence or neutron dose equivalent per x-ray absorbed dose with larger field sizes, but statistically there was no difference

Table 3: WPAFB Accelerator - Measurements on Table, 20 cm

Cnt #	Field Size [cm]	Loc'n [cm]	M.U.	Flux x 10^{-3} n/s-cm^2	Fluence x 10^{-6} n/cm^2	Dose [rem_n]	$mrem_n$/rad_x	Fluence/rad_x x 10^{-5}
141	10x10	20	200	694 ± 55	34.6 ± 2.7	0.823 ± 0.064	4.11 ± 0.32	1.73 ± 0.14
340	10x10	20	956	865 ± 54	155.7 ± 9.7	3.71 ± 0.23	3.88 ± 0.24	1.63 ± 0.10
336	20x16	20	955	901 ± 56	162.2 ± 10.8	3.86 ± 0.26	4.04 ± 0.27	1.70 ± 0.11
342	20x20	20	959	959 ± 60	172.6 ± 10.8	4.11 ± 0.26	4.29 ± 0.27	1.80 ± 0.11
346	20x20	20	956	956 ± 60	172.1 ± 10.8	4.10 ± 0.26	4.29 ± 0.27	1.80 ± 0.11

with different field sizes from this data. The average with a 10x10 cm field size was (1.472±0.025)x10^5 n/cm^2-rad_x ; with a 20x20 cm field size the average was (1.567±0.025)x10^5 n/cm^2-rad_x .

Table 4: WPAFB Accelerator - Measurements on Table, 30 cm

Cnt #	Field Size [cm]	Loc' [cm]	M.U.	Flux x 10^{-3} n/s-cm^2	Fluence x 10^{-6} n/cm^2	Dose [rem_n]	$mrem_n$/rad_x	Fluence/rad_x x 10^{-5}
145	10x10	30	200	611 ± 41	30.4 ± 2.0	0.724 ± 0.048	3.62 ± 0.24	1.52 ± 0.10
146	10x10	30	200	576 ± 38	28.7 ± 1.9	0.683 ± 0.045	3.42 ± 0.22	1.435 ± 0.095
338	10x10	30	958	778 ± 48	140.0 ± 8.6	3.33 ± 0.20	3.48 ± 0.21	1.461 ± 0.090
344	20x20	30	958	847 ± 53	152.5 ± 9.5	3.63 ± 0.22	3.79 ± 0.23	1.592 ± 0.099
348	20x20	30	957	820 ± 51	147.6 ± 9.2	3.51 ± 0.26	3.67 ± 0.27	1.542 ± 0.096

Table 5 gives measurements on the table when the flux integrators were centered 50 cm from the beam axis on the table. The trend of larger fluence/rad_x or $mrem_n/rad_x$ with larger field sizes reverses at this distance; the neutron fluence and neutron equivalent dose per x-ray absorbed dose decreases with larger field sizes. However, again there is no real difference statistically. At 10x10 cm field size the average is $(1.3043\pm0.0083)\times10^5$ $n/cm^2\text{-}rad_x$, and at 20x20 cm field size the average is $(1.2765\pm0.0075)\times10^5$ $n/cm^2\text{-}rad_x$.

Table 5: WPAFB Accelerator - Measurements on Table, 50 cm

Cnt #	Field Size [cm]	Loc' [cm]	M.U.	Flux x 10^{-3} $n/s\text{-}cm^2$	Fluence x 10^{-6} n/cm^2	Dose [rem_n]	$mrem_n/rad_x$	Fluence/ rad_x x 10^{-5}
142	10x10	50	200	528 ± 35	26.3 ± 1.8	0.626 ± 0.043	3.13 ± 0.22	1.315 ± 0.090
144	10x10	50	200	511 ± 35	26.2 ± 1.8	0.624 ± 0.043	3.12 ± 0.22	1.310 ± 0.090
341	10x10	50	956	684 ± 43	123.1 ± 7.7	2.93 ± 0.18	3.06 ± 0.19	1.288 ± 0.081
337	20x16	50	955	672 ± 42	121.0 ± 7.6	2.88 ± 0.18	3.02 ± 0.19	1.267 ± 0.080
343	20x20	50	959	684 ± 43	123.1 ± 7.7	2.93 ± 0.18	3.06 ± 0.19	1.284 ± 0.080
347	20x20	50	959	674 ± 42	121.3 ± 7.6	2.88 ± 0.18	3.01 ± 0.19	1.269 ± 0.079

The final table in this series, Table 6, gives results for on-table measurements when the flux integrators were centered 100 cm from the beam axis. The fluence per rad_x and $mrem_n$ per rad_x again show decreasing trends with larger field sizes, but statistically there is not a difference. At 10x10 cm field size the average was $(0.9315\pm0.0085)\times10^5$ $n/cm^2\text{-}rad_x$; at 20x20 cm field size the average was $(0.9025\pm0.0065)\times10^5$ $n/cm^2\text{-}rad_x$.

Table 6: WPAFB Accelerator - Measurements on Table, 100 cm

Cnt #	Field Size [cm]	Loc' [cm]	M.U.	Flux x 10^{-3} n/s-cm^2	Fluence x 10^{-6} n/cm^2	Dose [rem_n]	$mrem_n$/ rad_x	Fluence/ rad_x x 10^{-5}
147	10x10	100	200	381.3 ± 26.6	19.0 ± 1.3	0.452 ± 0.031	2.26 ± 0.16	0.940 ± 0.065
339	10x10	100	958	491 ± 31	88.4 ± 5.6	2.10 ± 0.13	2.19 ± 0.14	0.923 ± 0.058
345	20x20	100	958	484 ± 30	87.1 ± 5.4	2.07 ± 0.13	2.16 ± 0.14	0.909 ± 0.056
349	20x20	100	957	476 ± 30	85.7 ± 5.4	2.04 ± 0.13	2.13 ± 0.14	0.896 ± 0.056

These four tables (3-6) show the neutron fluence per photon rad to be within the range established by previous literature. Specifically, these measurements on the treatment table range from a high of $1.80x10^5$ n/cm^2-rad_x at 20 cm axial distance from the beam to a low of $8.96x10^4$ n/cm^2-rad^x at 100 cm axial distance from the beam, both at 20x20 cm field size. A range of $7.4x10^4$ n/cm^2-rad_x to $1.7x10^5$ n/cm^2-rad_x was expected from previous experiment, as from Table 16. There may be a trend between neutron measurements and field size. At closer distances there seem to be more neutrons released when the field size is increased, and at longer distances there seem to be fewer neutrons with a larger field size.

The next four tables (7-10) include more irradiations at the Varian Clinac 1800, again without patients. In these the flux integrators were not set on the treatment table. In the first two tables they were set on the medical stand next to the table, to simulate their placement during measurements with patients. Recall that this location is centered at 36.6 cm from the beam axis (Chapter III).

From Table 7 the neutron fluence averaged (1.149±0.018)x10^5 n/cm^2-rad_x at the side-of-table position for a 10x10 cm field size. For a 20x20 cm field size the fluence averaged (1.235±0.010)x10^5 n/cm^2-rad_x. In this case there is a statistical difference between the neutron fluence per rad_x for the different field sizes--the neutron fluence is higher for a larger field size.

Table 7: WPAFB Accelerator - Measurements Beside Table

Cnt #	Field Size [cm]	M.U.	Flux x 10^{-3} $n/s-cm^2$	Fluence x 10^{-6} n/cm^2	Dose [$mrem_n$]	$mrem_n$ / rad_x	Fluence/ rad_x x 10^{-5}
310	10x10	317	601 ± 39	36.1 ± 2.3	859 ± 55	2.71 ± 0.17	1.139 ± 0.073
311	10x10	316	624 ± 39	37.4 ± 2.3	890 ± 55	2.82 ± 0.17	1.184 ± 0.073
312	10x10	316	653 ± 41	39.2 ± 2.5	933 ± 56	2.95 ± 0.18	1.124 ± 0.079
313	20x20	318	667 ± 44	40.0 ± 2.6	952 ± 62	2.99 ± 0.19	1.258 ± 0.082
314	20x20	313	656 ± 41	39.4 ± 2.5	938 ± 56	3.00 ± 0.18	1.259 ± 0.080
315	20x20	318	647 ± 41	38.8 ± 2.5	923 ± 56	2.90 ± 0.18	1.220 ± 0.079
320	20x20	1914	652 ± 40	235 ± 14	5590 ± 330	2.92 ± 0.17	1.228 ± 0.073
324	20x20	1917	645 ± 40	232 ± 14	5520 ± 330	2.88 ± 0.17	1.210 ± 0.073

Table 8 is the same as Table 7, except a steel wedge and a lead block were used to shape the beam, as is often done in treatment. Count numbers 316 and 317 were done with a 45° steel wedge in the gantry head. Count numbers 318, 319, and 328 were done with a half-beam lead block set at 0° orientation in the gantry head. These data average (1.164±0.025)x10^5 n/cm^2-rad_x for the steel wedge, and (1.265±0.018)x10^5

$n/cm^2\text{-}rad_x$ for the lead block. There is no statistical difference between each of these averages and the average for the same condition without a wedge or block (Table 7), though the trend seems to be fewer neutrons with the steel wedge and more neutrons with the lead block. However there is a statistical difference between using the block and using the wedge; the difference in the averages is $(0.086 \pm 0.021) \times 10^5$ $n/cm^2\text{-}rad_x$.

Table 8: WPAFB Accelerator - Measurements Beside Table with Steel or Lead Beam Shapers; 20x20 cm Field Size

Cnt #	Beam Shaper	M.U.	Flux x 10^{-3} $n/s\text{-}cm^2$	Fluence x 10^{-6} n/cm^2	Dose [$mrem_n$]	$mrem_n$ / rad_x	Fluence/ rad_x x 10^{-5}
316	45° steel wedge	317	602 ± 40	36.1 ± 2.4	859 ± 57	2.71 ± 0.18	1.139 ± 0.076
317	45° steel wedge	318	630 ± 40	37.8 ± 2.4	900 ± 57	2.83 ± 0.18	1.189 ± 0.075
318	Pb block	316	677 ± 44	40.6 ± 2.6	966 ± 62	3.06 ± 0.20	1.285 ± 0.082
319	Pb block	318	679 ± 43	40.7 ± 2.6	969 ± 62	3.07 ± 0.19	1.280 ± 0.082
328	Pb block	1913	654 ± 41	235 ± 15	5590 ± 360	2.92 ± 0.19	1.229 ± 0.078

In Table 9 the flux integrators were set along a line perpendicular to both the axis of the table and the axis of the x-ray beam. These were at 2 and 4 meters from the center of the table. The measurements located at "2, wall" were set at 2 meters towards the far wall of the treatment room, as described in Table 2 in chapter 3. Those located at "2, door" and "4, door" were set 2 meters and 4 meters, respectively, towards the door of the treatment room. Additionally count numbers 329-331 were done with the lead block in the gantry head, as mentioned in the previous table. No statistical difference in the measurements

could be seen from these data with the inclusion of the lead block. There were more neutrons measured towards the wall of the treatment room than towards the door; one would expect more neutron reflection on that side since the corner of the room and the walls are closer on that side.

Table 9: WPAFB Accelerator - Measurements Off Table

Cnt #	Field Size [cm]	Loc'n [m]	M.U.	Flux x 10^{-3} n/s-cm^2	Fluence x 10^{-6} n/cm^2	Dose [mrem$_n$]	mrem$_n$ / rad$_x$	Fluence/ rad$_x$ x 10^{-4}
321	20x20	2, wall	1914	270 ± 17	97.2 ± 6.1	2310 ± 150	1.207 ± 0.078	5.08 ± 0.32
325	20x20	2, wall	1917	278 ± 18	100.1 ± 6.5	2380 ± 150	1.242 ± 0.078	5.22 ± 0.34
329	20x20	2, wall	1913	290 ± 18	104.4 ± 6.5	2480 ± 150	1.296 ± 0.078	5.46 ± 0.34
322	20x20	2, door	1914	220 ± 14	79.2 ± 5.0	1880 ± 120	0.982 ± 0.063	4.14 ± 0.26
326	20x20	2, door	1917	227 ± 14	81.7 ± 5.0	1940 ± 120	1.012 ± 0.063	4.26 ± 0.26
330	20x20	2, door	1913	228 ± 14	82.1 ± 5.0	1950 ± 120	1.019 ± 0.063	4.29 ± 0.26
323	20x20	4, door	1914	109.0 ± 7.2	39.2 ± 2.5	933 ± 60	0.487 ± 0.031	2.05 ± 0.13
327	20x20	4, door	1917	95.3 ± 6.3	34.3 ± 2.3	816 ± 55	0.426 ± 0.029	1.79 ± 0.12
331	20x20	4, door	1913	99.6 ± 6.5	35.6 ± 2.3	847 ± 55	0.443 ± 0.029	1.86 ± 0.12

Table 10, the final table in this section, presents results of flux integrator measurements with patients during their cancer therapy. The conditions were necessarily less well controlled for these measurements than for those without patients. The field sizes were not constant; a variety of lead blocks were used to shape the x-ray beam for individual treatments; the exposure times were short in comparison to the measurements without patients; the position of the flux integrators was less

well controlled. For instance, count #298 was placed by the patient's calf rather than beside the treated area because of treatment conditions (the gantry had to rotate around the table and the flux integrator had to be kept out of the way); this gave a lower neutron dose rate for this measurement, since the flux integrator was further away than in other measurements. For the other measurements the neutron equivalent dose per x-ray absorbed dose ($mrem_n/rad_x$) results vary somewhat, but is of the same order of magnitude as the without-patients measurements. This demonstrates the validity of this technique for measuring neutron dose for x-ray treatments at the WPAFB facility.

Table 10: WPAFB Accelerator - Measurements with Patients

Cnt #	Field Size [cm]	Monitor Units	Flux x 10^{-3} n/s-cm^2	Fluence x 10^{-6} n/cm^2	Dose [$mrem_n$]	$mrem_n$ / rad_x
149		294	852 ± 55	47.0 ± 3.0	1119 ± 71	3.81 ± 0.24
150		200	470 ± 33	18.0 ± 1.3	428 ± 31	2.14 ± 0.16
151		238	679 ± 45	30.1 ± 2.0	716 ± 48	3.01 ± 0.20
152		318	924 ± 60	44.4 ± 2.9	1057 ± 69	3.32 ± 0.22
298	8x8	243	26.1 ± 3.9	2.79 ± 0.42	66.4 ± 1.0	0.2733 ± 0.0041
299	14x25, 15x25	238	641 ± 40	28.8 ± 1.8	685 ± 43	2.88 ± 0.18
307	10x17, 12x17	199	682 ± 43	25.8 ± 1.6	614 ± 38	3.09 ± 0.19
300	17x17, 14x17	258	358 ± 23	17.6 ± 1.1	419 ± 26	1.62 ± 0.10
308	17x17, 14x17	258	380 ± 24	18.9 ± 1.2	450 ± 29	1.74 ± 0.11
301	17x20, 16x20	220	607 ± 39	24.8 ± 1.6	590 ± 38	2.68 ± 0.17
309	17x20, 16x20	220	463 ± 29	19.4 ± 1.2	462 ± 29	2.10 ± 0.13

From Table 10 it is seen the neutron equivalent dose per x-ray absorbed dose varied from a low of 1.62 $mrem_n/rad_x$ to a high of 3.81 $mrem_n/rad_x$, or dose to patient of 0.42 to 1.12 rem_n .

Kettering CGM Saturne 1 Measurements

A series of measurements were also made at Kettering Memorial Hospital. The Kettering x-ray machine is a French-made CGM Saturne 1, which operates at 10 MV. It is magnetron driven, with a beam energy of 14-15 MeV. It has a lead collimator, so a flux-to-dose conversion factor of 4.17×10^{-8} rem_n-cm^2/neutron was used. The setup was essentially identical to that done at the WPAFB Medical Center.

Tables 11-14, following, give the results of a series of measurements at Kettering Memorial Hospital. The tables give measurements at 20, 30, 50, and 100 cm on the treatment table, along its axis. The CMG Saturne 1 was run at 1500 monitor units, so the doses were all divided by 1500 to obtain the relation between $mrem_n$ and rad_x.

Table 11 is for the measurements at 20 cm. Two field sizes, 10x10 cm and 20x20 cm, were used. The measurements of fluence/rad_x and $mrem_n/rad_x$ were statistically larger for the larger field size at this distance: averages were $(5.11 \pm 0.21) \times 10^4$ n/cm^2-rad_x for 10x10 cm field size vs. $(5.985 \pm 0.035) \times 10^4$ n/cm^2-rad_x for 20x20 cm field size. It seems neutrons may be blocked at closer distances by a smaller field size.

Table 12 gives measurements at 30 cm axial distance on the treatment table. Again, measurements were made with field sizes at both 10x10 cm and 20x20 cm. The larger field size again gives larger values for the neutron measurements per x ray. Averages were $(4.72 \pm 0.06) \times 10^4$ n/cm^2-rad_x at 10x10 cm and $(5.18 \pm 0.16) \times 10^4$ n/cm^2-rad_x at 20x20 cm.

Table 11: Kettering CGM Saturne 1 - Measurements on Table, 20 cm

Cnt #	Field Size [cm]	Loc'n [cm]	Flux x 10^{-3} n/s-cm^2	Fluence x 10^{-6} n/cm^2	Dose [rem$_n$]	mrem$_n$/ rad$_x$	Fluence/ rad$_x$ x 10^{-4}
350	10x10	20	198.4 ± 3.6	73.6 ± 1.3	3.069 ± 0.054	2.046 ± 0.036	4.907 ± 0.087
355	10x10	20	215.3 ± 3.9	79.8 ± 1.4	3.328 ± 0.058	2.219 ± 0.039	5.320 ± 0.093
362	20x20	20	243.5 ± 4.8	90.3 ± 1.8	3.766 ± 0.075	2.511 ± 0.050	6.02 ± 0.12
370	20x20	20	240.9 ± 4.5	89.3 ± 1.7	3.724 ± 0.071	2.483 ± 0.047	5.95 ± 0.11

Table 12: Kettering CGM Saturne 1 - Measurements on Table, 30 cm

Cnt #	Field Size [cm]	Loc'n [cm]	Flux x 10^{-3} n/s-cm^2	Fluence x 10^{-6} n/cm^2	Dose [rem$_n$]	mrem$_n$/ rad$_x$	Fluence/ rad$_x$ x 10^{-4}
353	10x10	30	193.3 ± 3.6	71.7 ± 1.3	2.990 ± 0.054	1.993 ± 0.036	4.780 ± 0.087
359	10x10	30	188.6 ± 3.6	69.9 ± 1.3	2.915 ± 0.054	1.943 ± 0.037	4.660 ± 0.087
366	20x20	30	216.2 ± 4.2	80.2 ± 1.6	3.344 ± 0.067	2.229 ± 0.045	5.347 ± 0.011
374	20x20	30	203.1 ± 4.2	75.3 ± 1.6	3.140 ± 0.067	2.093 ± 0.045	5.020 ± 0.011

Table 13 shows measurements when the flux integrators were centered 50 cm from the beam axis on the table. Both 10x10 cm and 20x20 cm field sizes were used. At this distance, however, there was no statistical difference in the neutron measurements per rad x-ray with varying field size. Perhaps neutron scatter and reflection has begun to become more uniform with larger distances from the target.

Table 13: Kettering CGM Saturne 1 - Measurements on Table, 50 cm

Cnt #	Field Size [cm]	Loc'n [cm]	Flux x 10^{-3} n/s-cm^2	Fluence x 10^{-6} n/cm^2	Dose [rem_n]	$mrem_n$/ rad_x	Fluence/ rad_x x 10^{-4}
351	10x10	50	161.6 ± 3.3	59.9 ± 1.2	2.498 ± 0.050	1.665 ± 0.033	3.993 ± 0.080
358	10x10	50	161.6 ± 3.3	59.9 ± 1.2	2.498 ± 0.050	1.665 ± 0.033	3.993 ± 0.080
363	20x20	50	166.6 ± 3.6	61.8 ± 1.3	2.577 ± 0.054	1.718 ± 0.036	4.120 ± 0.087
371	20x20	50	156.2 ± 42	57.9 ± 1.2	2.414 ± 0.050	1.609 ± 0.033	3.860 ± 0.080

Table 14 gives the on-table measurements when the flux integrator was centered 100 cm from the beam axis. Here the trend seems to agree with the WPAFB measurements, in that the neutron fluence and equivalent dose per x-ray absorbed dose decreased with a larger field size at the further distances. The statistical difference is not strong, however, based on this data. The averages were $(2.99\pm0.14)\times10^4$ n/cm^2-rad_x and $(2.720\pm0.048)\times10^4$ n/cm^2-rad_x at 10x10 cm and 20x20 cm respectively.

For a 10 MV x-ray machine a neutron fluence to photon dose measurement on the order of 1×10^4 n/cm^2-rad_x would be expected from Table 16. Table 11 shows averages of $(5.11\pm0.21)\times10^4$ n/cm^2-rad_x for a 10x10 cm field and $(5.985\pm0.035)\times10^4$ n/cm^2-rad_x for a 20x20 cm field, both at 20 cm distance from the beam. These are perhaps 3½ times larger than expected, but only a limited number of references for 10 MV accelerators were included. Without more knowledge of typical 10 MV accelerators it cannot be said here whether these are truly larger measurements than the norm. This accelerator does produce a lower fluence per x-ray dose than the WPAFB accelerator.

Table 14: Kettering CGM Saturne 1 - Measurements on Table, 100 cm

Cnt #	Field Size [cm]	Loc'n [cm]	Flux x 10^{-3} n/s-cm^2	Fluence x 10^{-6} n/cm^2	Dose [rem$_n$]	mrem$_n$/ rad$_x$	Fluence/ rad$_x$ x 10^{-4}
352	10x10	100	115.3 ± 2.6	42.75 ± 0.96	1.728 ± 0.040	1.152 ± 0.027	2.850 ± 0.064
354	10x10	100	126.3 ± 2.7	46.8 ± 1.0	1.952 ± 0.042	1.301 ± 0.028	3.120 ± 0.067
367	20x20	100	111.9 ± 2.8	41.5 ± 1.0	1.731 ± 0.042	1.154 ± 0.028	2.767 ± 0.067
375	20x20	100	108.1 ± 2.5	40.08 ± 0.93	1.671 ± 0.039	1.114 ± 0.026	2.672 ± 0.062

Table 15 includes more measurements done at the Kettering accelerator. Measurements at 200 and 400 cm distance from the beam axis were done perpendicularly to the table axis, with the flux integrators placed on chairs. The measurements at 2 meters were done with the bottom of the flux integrator at 62.5 cm above the floor. At 4 meters, count number 356 was done with the bottom of the flux integrator at 61.5 cm from the floor; count number 357 was done with the bottom of the flux integrator at 60.5 cm above the floor. All other measurements at 4 meters were done with the bottom of the flux integrators at 62.5 cm above the floor. Unfortunately the height of the accelerator head target is unknown to this researcher, so the straight line distance from the target to the foils within the flux integrators could not be calculated. These measurements are included for comparison only. There seems to be a trend of higher neutron measurements at smaller field sizes, consistent with the trends seen at 50 and 100 cm on the table. However no statistical difference between the field sizes could be shown. Averages at 200 cm were (1.344±0.049)x10^4 n/cm^2-rad$_x$ at 10x10 cm

Table 15: Kettering CGM Saturne 1 - Measurements Off Table

Cnt #	Field Size [cm]	Loc'n [cm]	Flux x 10^{-3} n/s-cm^2	Fluence x 10^{-6} n/cm^2	Dose [rem_n]	$mrem_n$/ rad_x	Fluence/ radx x 10^{-4}
356	10x10	200	56.3 ± 1.6	20.90 ± 0.59	0.872 ± 0.025	0.581 ± 0.017	1.393 ± 0.039
360	10x10	200	52.4 ± 1.5	19.43 ± 0.56	0.810 ± 0.023	0.540 ± 0.015	1.295 ± 0.037
364	20x20	200	49.9 ± 1.5	18.50 ± 0.56	0.771 ± 0.023	0.514 ± 0.015	1.233 ± 0.037
368	20x20	200	50.9 ± 1.5	18.87 ± 0.56	0.787 ± 0.023	0.525 ± 0.015	1.259 ± 0.037
372	20x20	200	50.4 ± 1.5	18.69 ± 0.56	0.779 ± 0.023	0.519 ± 0.015	1.246 ± 0.037
376	20x20	200	48.7 ± 1.8	18.06 ± 0.67	0.753 ± 0.028	0.502 ± 0.019	1.204 ± 0.045
357	10x10	400	23.6 ± 1.1	58.75 ± 0.41	0.365 ± 0.017	0.243 ± 0.011	5.833 ± 0.027
361	10x10	400	25.6 ± 1.2	9.49 ± 0.44	0.396 ± 0.018	0.264 ± 0.012	6.327 ± 0.029
365	20x20	400	21.6 ± 1.1	8.01 ± 0.41	0.334 ± 0.017	0.223 ± 0.011	5.340 ± 0.027
369	20x20	400	23.2 ± 1.1	8.60 ± 0.41	0.359 ± 0.017	0.239 ± 0.011	5.733 ± 0.027
373	20x20	400	24.5 ± 1.2	9.08 ± 0.44	0.379 ± 0.018	0.253 ± 0.012	6.053 ± 0.029
377	20x20	400	22.8 ± 1.2	8.45 ± 0.44	0.352 ± 0.018	0.235 ± 0.012	5.633 ± 0.029

and $(1.235\pm0.012)\times10^4$ n/cm^2-rad_x at 20x20 cm. At 400 cm the averages were $(6.08\pm0.25)\times10^4$ n/cm^2-rad_x at 10x10 cm and $(5.69\pm0.15)\times10^4$ n/cm^2-rad_x at 20x20 cm.

V Conclusion

Summary

The first step in this project was using the standard graphite pile to ascertain the counting efficiency of the Geiger-Mueller detector used to count activated gold foils. Foils with a nominal thickness of 0.5 mil were irradiated and counted individually and in stacks of two and three (to make nonimal thicknesses of 1 mil and 1.5 mil) to give a graph of counts vs. thickness. The resulting exponential relation was combined with a series of cadmium-difference measurements to obtain the relation for efficiency, ϵ, to use when counting foil activity with the detector. This relation was found to be

$$\epsilon = (0.428 \pm 0.021)\exp[(-0.01045 \pm 0.00031)x] \qquad (24)$$

where x has units of mg/cm^2 . The efficiency term ϵ is unitless.

The next major step was calibration of the flux integrators. A series of measurements at various heights above the concrete platform in the AFIT reactor dome gave the relation

$$\phi = (2970 \pm 180)S_{\circ} \qquad (28a)$$

which was used for all subsequent irradiations made with gold foils in the flux integrators. $S_{\circ}$ has units of $[mg^{-1}s^{-1}]$. It is derived from $S_{\circ} = A_{\circ}/Mass$ where

$$A_\infty = \frac{\lambda C_{net} e^{\lambda t_w}}{\epsilon(1-e^{-\lambda t_c})(1-e^{-\lambda t_e})} \qquad (10)$$

and t_e, t_c, and t_w are the exposure time, count time, and wait time of the gold foil, respectively. To complete the summary of important equations the relation $A_\infty = C_s/\epsilon$ is repeated, where

$$C_s = \frac{\lambda C_{net} e^{\lambda t_w}}{(1-e^{-\lambda t_c})(1-e^{-\lambda t_e})} \qquad (18)$$

Both A_∞ and C_s have units of $[s^{-1}]$.

The final part of this thesis study involved measurements done with the flux integrators without and with patients present at the WPAFB Varian Clinac 1800 x-ray therapy machine. Measurements were also done at the Kettering CGM Saturne 1 10 MV cancer therapy machine for comparison.

Results and Further Suggestions

In the saturation activity equation and saturation-to-flux equation developed here, the constants for detector efficiency ϵ and flux integrator calibration constant K were not significantly different from those determined in the previous work by Rossano. This confirms the stability of the measuring system developed by him and gives greater confidence of its validity and usefulness.

Application of the procedure at the Varian Clinac 1800 at the WPAFB Medical Center gave fluences within the range of previously published results, as in Table 16. Application at the CGM Saturne 1 at Kettering

Memorial Hospital further proved the usability of this scheme. The procedure outlined here should be quite feasible for periodic monitoring of the neutron flux of the accelerator at the WPAFB Medical Center.

Flux integrator irradiations at the WPAFB Medical Center without patients gave $(1.80\pm0.11)\times10^5$ $n/cm^2\text{-}rad_x$ for measurements on the treatment table, 20 cm from the beam axis, with a field size of 20x20 cm. The corresponding average neutron equivalent dose per x-ray absorbed dose was 4.290 ± 0.010 $mrem_n/rad_x$. Measurements at a position immediately beside the treatment table averaged $(1.235\pm0.035)\times10^5$ $n/cm^2\text{-}rad_x$ with a field size of 20x20 cm; the corresponding average neutron equivalent dose per x-ray absorbed dose was 2.938 ± 0.080 $mrem_n/rad_x$. Measurements were also done at 30, 50, and 100 cm from the beam axis on the treatment table, as well as 2 meters from the beam axis on either side of the table and at 4 meters from the beam axis towards the door of the treatment room.

Based on the measurements at different locations with different field sizes, there seems to be an interesting trend. For measurements done closer than about 40 cm from the beam axis, there is a larger neutron fluence with larger field size. For measurements at 50 cm and further, there is a larger neutron fluence with smaller field size. A smaller field size means there is more material in the path of the beam; we might expect more neutrons to be released. However, this same material seems to deflect neutrons from the area close to it. This could explain why there are fewer neutrons measured close to the beam and more further away when the field size is reduced.

The difference in fluence/rad_x between the steel wedge and the lead block (Table 8) suggests it might be safer to the patient to use steel

for beam shaping. However, a variety of factors which surely contributed to the difference between the lead and steel (mass, neutron binding energies, etc.) are not addressed here.

Flux integrator measurements were also done during patient therapy at the WPAFB Medical Center. These resulted in measurements ranging from 1.62±0.10 $mrem_n/rad_x$ to 3.81±0.24 $mrem_n/rad_x$ (corresponding to 0.42 rem_n and 1.12 rem_n dose to the patient), with a variety of field sizes based on the particular prescribed treatments. These measurements are in the range of the measurements done without patients, and all measurements compare well with similar studies in the literature.

Future investigation might focus on the calculation of the efficiency of the detector(s) used to count activated foils. The procedure used here may be more cumbersome than is desired or necessary. If a gamma counting system is used instead of a beta counting system, the dependency on foil thickness may be neglected for foils of similar thickness since gammas are attenuated much less than betas. A future system might also be developed without needing to use the standard graphite pile for calibration: foils might be irradiated in the flux integrators using a known neutron flux (as was done here in the reactor dome) and the resulting activation compared with this known flux to calibrate the counting system.

In this paper the saturation specific activity S_∞ was used instead of simply the saturation activity A_∞ often cited in the literature. The saturation specific activity was used to account for the differences in the foils since their masses and thicknesses varied within a small range. Again, if future work uses a gamma counter, these differences may prove to be negligible if foils sufficiently thin are used. In that case there may be no need to account for the differences, as was done

here.

As for the topic of this thesis, the measurement of extraneous neutrons from x-ray cancer therapy is important and relevant both for its own inherent interest and for its contribution to improvements in health care. The author hopes that this study has, in some way, made a contribution to the universal good.

Appendix A: Neutron Dose Conversion Factors

A number of studies have been done which relate neutron fluence to photon dose, neutron dose to photon dose, and neutron fluence to neutron dose. These relations are usually based on the average energy of the neutron spectrum, which in turn depends on the photon energy and the target, flattener, and collimator assembly materials.

For comparison and reference a table of conversion factors from the literature follows, sorted by units. The references are given at the end of part d. For reference d, the accelerator voltage is given instead of the photon energy in the fourth column of parts a-c.

Table 16: Various Neutron Dose Conversion Factors

a. Assorted Units

Factor	Units	Spectrum or Loc'n	Photon Energy	Machine	Reference
6.03×10^{-5}	rad_n/rad_x	Fast	10 MeV	V-C 18	(a: 400)
5.5×10^{-7}	rad_n/rad_x	Thermal	10 MeV	V-C 18	(a: 400)
1.2×10^{-5}	rad_n/rad_x	Thermal	18 MV	V-C 20	(d: 673)
4.38	$mrem_n/rad_x$	in-beam	16 MeV	SL75-20 linac	(c: 109)
1.5	$mrem_n/rad_x$		45 MeV	BBC Betatron	(g: 55)
0.122	$(mrem/hr)/(n/cm^2\text{-}s)$	^{252}Cf			(a: 399)

b. Neutron Fluence per Photon Rad

Factor	Units	Spectrum or Loc'n	Photon Energy	Machine	Reference
$8x10^4$	$n/cm^2\text{-}rad_x$	Fast	18 MV	Varian linac	(d: 673)
$1.2x10^3$	$n/cm^2\text{-}rad_x$	Thermal	10 MeV	V-C 18	(a: 400)
$1.8x10^5$	$n/cm^2\text{-}rad_x$	Fast	33 MeV	BBC Betatron	(e: 400)
$1.8x10^5$	$n/cm^2\text{-}rad_x$	Fast	18 MV	V-C 20	(d: 673)
$2.7x10^4$	$n/cm^2\text{-}rad_x$	Thermal	18 MV	V-C 20	(d: 673)
$1.52x10^4$	$n/cm^2\text{-}rad_x$	Fast 5 cm out	10 MeV	V-C 18	(a: 400)
$1.6x10^{10}$	$n/\text{-}rad_x$	infinite target	25 MeV		(b: 82)
$4.2x10^8$	$n/\text{-}rad_x$	infinite target	10 MeV	V-C 18	(b: 83)
$2.1x10^5$	$n/cm^2\text{-}rad_x$		25 MeV		(b: 84)
$1.5x10^5$	$n/cm^2\text{-}rad_x$	out of beam	16 MeV	SL75-20 linac	(c: 116)
$7.2x10^4$	$n/cm^2\text{-}rad_x$	out of beam	16 MeV	MEL linac	(e: 400)
$1.7x10^5$	$n/cm^2\text{-}rad_x$	5 cm out of beam	19 MeV	Siemens Betatron	(e: 400)

c. Rad Neutron Dose per Neutron Fluence

Factor	Units	Spectrum	Photon Energy	Machine	Reference
$3.97x10^{-9}$	$rad_n\text{-}cm^2/n$	^{252}Cf			(a: 399)
$4.57x10^{-10}$	$rad_n\text{-}cm^2/n$	Thermal	10 MeV	V-C 18	(a: 399
$4.4x10^{-10}$	$rad_n\text{-}cm^2/n$	Thermal	18 MV	V-C 20	(d: 673)
$3.0x10^{-9}$	$rad_n\text{-}cm^2/n$	^{252}Cf			(e: 400)
$2.74x10^{-11}$	$rad_n\text{-}cm^2/n$	Thermal			(f: 467)

d. Rem Neutron Dose per Neutron Flux

Factor	Units	Spectrum	Photon Energy	Material	Reference
4.2×10^7	$n\text{-}rem_n/cm^2$	$\bar{E}$ = 1 MeV		Tungsten	(b: 77)
2.4×10^7	$n\text{-}rem_n/cm^2$	$\bar{E}$ = 2 MeV		Lead	(b: 77)

V-C refers to Varian Clinac machines.

References:
a: (McGinley et al, 1976)
b: (McCall and Swanson, 1979)
c: (Axton and Bardell, 1975)
d: (Purdy and Glasgow, 1984)
e: (Wilenzick et al, 1973)
f: (Attix, 1986)
g: (Rossano, 1989)

From the last two entries of part b. of the preceding table, it is reasonable to expect between 7.2×10^4 $n/cm^2\text{-}rad_x$ and 1.7×10^5 $n/cm^2\text{-}rad_x$ for the Varian Clinac 1800. Based on an average neutron energy of approximately 1 MeV for tungsten photoneutrons (Toms and Stephens, 1957: 77-81) a conversion factor of 2.38×10^{-8} rem-n/cm^2 was used for neutron flux to dose calculations for the Varian Clinac 1800 (McCall and Swanson, 1979: 77). If the predominate material in the accelerator head were lead (as with the CGM Saturne 1 accelerator at Kettering), the average photoneutron energy would be about 2 MeV (NCRP 79, 1979: 30) and a factor of 4.17×10^{-8} rem-n/cm^2 would be appropriate for the neutron flux to neutron dose conversion factor. (NCRP 79, 1979: 45; McCall and Swanson, 1979: 77). Note these two conversion factors are the inverse of the factors in part d. of the above table.

Once the neutron fluence is known, then, the neutron dose can be calculated by the formula

$$H = \left(2.38 \times 10^{-8} rem_{n_0}^{1} n/cm^2\right)\Phi \qquad (16)$$

for the neutrons from the WPAFB electron accelerator, which uses tungsten. At Kettering Memorial Hospital the formula is

$$H = \left(4.17 \times 10^{-8} rem_{n_0}^{1} n/cm^2\right)\Phi \qquad (17)$$

since the CGM Saturne 1 uses lead.

Appendix B: Foil Parameters

The list which follows describes each of the foils used for this report.

Foil Number	Mass [mg]	Diameter [cm]	Thickness [mg/cm^2]
1	125.1	1.281	97.1
2	131.1	1.277	102.4
3	134.9	1.287	103.4
4	130.1	1.288	99.9
5	135.9	1.279	105.8
6	135.3	1.288	103.8
7	132.2	1.288	101.5
8	128.8	1.288	98.9
15	136.9	1.280	106.4
16	127.1	1.290	97.2
17	125.0	1.282	96.8
18	124.8	1.278	97.3
19	128.9	1.281	100.0
20	131.9	1.277	103.0
21	133.8	1.276	104.6
22	254.0	2.555	49.5
23	242.9	2.555	47.4
24	253.2	2.547	49.7
25	246.0	2.552	48.1
26	249.2	2.553	48.7
27	255.5	2.552	50.0
28	250.6	2.552	49.0
29	240.0	2.549	47.0

Foil Number	Mass [mg]	Diameter [cm]	Thickness [mg/cm^2]
30	251.2	2.550	49.2
31	248.5	2.559	48.3
32	244.9	2.550	48.0
33	249.6	2.553	48.8
34	242.3	2.560	47.1
35	245.3	2.553	47.9
36	291.6	2.546	57.3
37	259.6	2.548	50.9
38	273.3	2.557	53.2
39	278.0	2.551	54.4
40	267.4	2.554	52.2
41	256.8	2.550	50.3
42	286.4	2.555	55.9
43	257.3	2.549	50.4
44	287.6	2.552	56.2
45	265.9	2.554	51.9
46	278.7	2.566	53.9
47	271.9	2.566	52.6
48	271.9	2.541	53.6
49	300.7	2.547	59.0
50	279.0	2.560	54.2
51	281.0	2.555	54.8
52	266.5	2.541	52.6
53	266.6	2.540	52.6
54	266.2	2.541	52.5
55	266.4	2.543	52.5
56	276.3	2.573	53.1

Foil Number	Mass [mg]	Diameter [cm]	Thickness [mg/cm^2]
57	299.7	2.575	57.5
58	264.1	2.593	50.0
59	273.4	2.571	52.7
60	273.3	2.580	52.3
61	309.5	2.578	59.3
62	262.8	2.594	49.7
63	270.2	2.562	52.4
64	275.0	2.577	52.7
65	306.0	2.583	58.4
66	298.1	2.577	57.2
67	310.0	2.584	59.1
68	310.5	2.576	59.6
69	309.5	2.586	58.9
70	271.9	2.582	51.9
71	276.5	2.579	52.9
72	278.9	2.575	53.6
73	272.2	2.559	52.9
74	301.8	2.574	58.0
75	272.2	2.571	52.4
76	267.1	2.584	50.9
77	278.4	2.581	53.2
78	267.3	2.550	52.3
79	285.9	2.555	55.8
80	287.1	2.551	56.2
81	266.1	2.547	52.2

Foil Number	Mass [mg]	Diameter [cm]	Thickness [mg/cm^2]
82	298.0	2.540	58.8
83	294.5	2.541	58.1
84	263.1	2.561	51.1
J-01	119.5	2.558	23.3
J-02	122.9	2.529	24.5
J-03	122.9	2.560	23.8
J-04	481.5	2.493	98.6
J-05	496.5	2.531	98.7
J-06	468.1	2.490	96.1

Appendix C: Increase in M580 and M1170 Outputs

The equation for computing the output of a Pu-Be source is

$$Q(t) = \alpha_1 \lambda_1 N_1 e^{-\lambda_1 t} + \alpha_2 \lambda_2 N_2 e^{-\lambda_2 t} + \alpha_4 \lambda_4 N_4 e^{-\lambda_4 t}$$
$$+ \alpha_4 \lambda_4 N_3 \frac{\lambda_3}{\lambda_4 - \lambda_3} (e^{-\lambda_3 t} - e^{-\lambda_4 t}) \qquad (29)$$

where α is the average neutron yield per alpha particle, λ is the disintegration constant, N is the number of atoms at time t=0, and the subscripts 1, 2, 3, and 4 refer to ^{239}Pu, ^{240}Pu, ^{241}Pu, and ^{241}Am respectively (Anderson, 1968:142). For most such neutron sources - as is true of M580 and M1170, used in this thesis project - the amount of ^{241}Am is negligible or non-existent at time t=0; thus N_4=0 and the third term above goes to zero. Also the decay of ^{239}Pu and ^{240}Pu is very small so that the exponentials in the first two terms are approximately unity. They can be combined into

$$Q(0) = \alpha_1 \lambda_1 N_1 + \alpha_2 \lambda_2 N_2 \qquad (30)$$

which is the initial emission rate given for the source (Anderson, 1968:143). With these simplifications Eq (29) above may be written as

$$Q(t) = Q(0) + \alpha_4 \lambda_4 N_3 \frac{\lambda_3}{\lambda_3 - \lambda_4} (e^{-\lambda_4 t} - e^{-\lambda_3 t}) \qquad (31)$$

Now $\lambda_3 = 4.83 \times 10^{-2}$ yr^{-1} and $\lambda_4 = 1.60 \times 10^{-3}$ yr^{-1} (Chart of Nuclides,

1983:47) and a_4=52x10^{-6} neutrons/α (Mound, 1962:F-7). Also N_3 may be written as

$$N_3 = M p_3 \frac{N_a}{AW_3} \tag{32}$$

where M is the total mass of Pu in the source, p_3 is the fraction of the mass which is ^{241}Pu, N_a is Avogadro's number, and AW_3 is the atomic weight of ^{241}Pu. Substituting these values and making appropriate conversions (such as years to seconds) gives

$$Q(t) = Q(0) + 6.84 x 10^6 M p_3 (e^{-\lambda_3 t} - e^{-\lambda_4 t}) \tag{33}$$

in units of neutrons/second.

For neutron source M580, the variables have the following values:

$Q(0)$ = 8.86x10^6 n/s on 23 June 1960

t = 29.19 years on 1 September 1989

M = 79.79 g

p_3 = 0.0044

(Mound, 1960:1; Anderson, 1967:145; 1980:429). Substituting these values into Eq (33) gives $Q(t)$ = 1.06x10^7 n/s as the output during the time of this thesis.

(A note on p_3 for M580 is in order here. The shipping data from Monsanto for M580 could not be found, so a specific reference for p_3 was not available to this researcher. Presumably Rossano had the reference

but it has since been lost. There are at least two ways to determine the value for p_3 for the time of this study, then. Using the value reported by Rossano for M580 at t=26.7 years, one could solve Eq (33) for p_3 since every other value was known. At t=26.7 years, Rossano reported $Q(t)=10.5 \times 10^6$ n/s (Rossano, 1989:64). Solving Eq (33) for p_3 gives 0.0044 . Another method is to compare the current output of M580 and M1170 to each other, as is done in Appendix G. The ratios of measured output compared with the ratios of calculated output from Eq (33) allows one to solve for p_3 for M580, with p_3 well known for M1170 but not so well known for M580. In addition to these calculations there are two literature references - (Anderson, 1967:145; 1980:429) - which lend support to this induced value of p_3 for M580.)

Since M580 is the neutron source for the standard graphite pile, an increase in its flux causes an increase in the thermal neutron flux of the pile. Dividing Q(t) by Q(0) gives the ratio $Q(t)/Q(0) = 1.193$, hence the assertion that the neutron output of PuBe source M580 has increased 19.3% since its birth (where t=29.19 years).

For neutron source M1170, the following values were used:

$Q(0) = 9.00 \times 10^6$ n/s on 2 March 1962

t = 27.38 years on 20 July 1989

M = 76.36 g

$p_3 = 0.0055$

(Mound, 1962:F-1). These values in Eq (33) give $Q(t) = 1.1 \times 10^7$ n/s for the output during the time of this thesis.

Appendix D: Foil Thickness vs Counts Data

The two table in this appendix give the data used for foil thickness dependency determination. Table 17 gives the data used in Figure 3, for saturation counts/thickness vs foil thickness. Table 18 gives the data used in Figure 4, the graph of saturation counts/mass vs foil thickness. The saturation counts (units [s^{-1}]) were computed by

$$C_s = \frac{\lambda C_{net} e^{\lambda t_w}}{(1 - e^{-\lambda t_s})(1 - e^{-\lambda t_c})} \qquad (18)$$

Thickness is in units of mg/cm^2 , and mass is in units of milligram.

Table 17: Data for Foil Thickness vs Saturation Counts/Thickness

Foil Count No.	Thickness, x [mg/cm^2]	C_s/x [$cm^2/mg-s$]
253	24.8	2.015 ± 0.020
254	24.8	1.995 ± 0.020
255	24.8	1.987 ± 0.020
256	24.8	2.007 ± 0.020
257	25	1.991 ± 0.020
258	25	2.021 ± 0.022
259	25	2.021 ± 0.020
260	24.9	2.002 ± 0.020
261	24.9	2.023 ± 0.024
262	24.9	1.977 ± 0.021
263	24.6	2.058 ± 0.021
264	24.6	2.049 ± 0.021
265	24.6	2.048 ± 0.021
266	49.8	1.515 ± 0.013
267	49.8	1.538 ± 0.014
268	74.7	1.1857 ± 0.0092
269	74.7	1.217 ± 0.011
272	49.5	1.518 ± 0.013
273	49.5	1.541 ± 0.015
274	74.5	1.1949 ± 0.0093
275	74.5	1.218 ± 0.011

Table 18: Data for Foil Thickness vs Saturated Counts/Mass

Foil Count No.	Thickness, x [mg/cm^2]	C_s/x [cm^2/mg-s]
253	24.8	1.542 ± 0.015
254	24.8	1.527 ± 0.015
255	24.8	1.521 ± 0.015
256	24.8	1.536 ± 0.015
257	25	1.518 ± 0.015
258	25	1.540 ± 0.016
259	25	1.540 ± 0.016
260	24.9	1.534 ± 0.016
261	24.9	1.550 ± 0.018
262	24.9	1.515 ± 0.016
263	24.6	1.549 ± 0.016
264	24.6	1.541 ± 0.016
265	24.6	1.541 ± 0.016
266	49.8	1.1572 ± 0.0097
267	49.8	1.175 ± 0.011
268	74.7	0.9066 ± 0.0071
269	74.7	0.9303 ± 0.0081
272	49.5	1.1523 ± 0.0097
273	49.5	1.170 ± 0.011
274	74.5	0.9084 ± 0.0070
275	74.5	0.9261 ± 0.0081

To show how these numbers were obtained, take Foil Count No. 253 in table 17. The values for each of the variables in Eq (18) are taken from Appendix I, which contains the data from each irradiation and count. For #253 the following values were used:

t_w = 8 minutes

t_e = 2875 minutes

t_c = 500 seconds

Cnet = 10175 - (500 s)(0.320 s^{-1} background) = 10015 counts

$t_{½}$ = 2.6935 days

λ = (ln2/2.6935 days) * (1 day/86400 seconds)

These values were substituted into the equation; the value of C_s thus obtained was divided by the value of the thickness in the second column, to give the value in the third column. All following values, and the values in the next table, were calculated similarly.

Appendix E: Detector Efficiency

The data for the graph in Figure 6 follow. This data was used to determine the constant f_x in Eq (23) for detector efficiency, ϵ.

Table 19: Cadmium Difference Pairs in Graphite Pile

Ser. No.	Str	B/C	$C_s \pm \sigma$	$\epsilon' \pm \sigma$	ϕf_x	ϕ
16	1	b	110.1 ± 1.2	0.5814 ± 0.0018	1658 ± 33	3854
19	1	c	41.00 ± 0.51	0.5694 ± 0.0018		
64	1	b	107.7 ± 1.4	0.5961 ± 0.0018	1673 ± 40	3854
82	1	c	38.04 ± 0.68	0.6037 ± 0.0019		
13	2	b	235.8 ± 1.7	0.5558 ± 0.0017	3239 ± 50	8256
22	2	c	91.82 ± 0.97	0.5771 ± 0.0018		
67	2	b	224.6 ± 2.0	0.6094 ± 0.0019	3489 ± 60	8256
85	2	c	83.3 ± 1.0	0.6056 ± 0.0019		
10	3	b	249.0 ± 1.7	0.5906 ± 0.0018	4050 ± 53	9449
25	3	c	82.9 ± 1.0	0.5711 ± 0.0018		
70	3	b	245.4 ± 2.1	0.5949 ± 0.0018	4084 ± 61	9449
88	3	c	77.38 ± 0.97	0.6005 ± 0.0019		
7	4	b	155.7 ± 1.3	0.5576 ± 0.0017	2870 ± 34	6824
28	4	c	32.37 ± 0.45	0.5398 ± 0.0017		
73	4	b	153.2 ± 1.6	0.6049 ± 0.0019	3125 ± 45	6824
91	4	c	27.59 ± 0.58	0.6113 ± 0.0019		
4	5	b	72.83 ± 0.93	0.5912 ± 0.0018	1647 ± 24	3794
31	5	c	5.98 ± 0.18	0.5676 ± 0.0018		
76	5	b	74.29 ± 0.95	0.6011 ± 0.0019	1696 ± 25	3794
94	5	c	6.04 ± 0.12	0.6062 ± 0.0019		
1	6	b	33.85 ± 0.63	0.5796 ± 0.0018	793 ± 16	1754
34	6	c	0.96 ± 0.10	0.5640 ± 0.0017		
79	6	b	34.48 ± 0.65	0.5930 ± 0.0018	825 ± 16	1754
97	6	c	1.052 ± 0.041	0.5495 ± 0.0017		

For the above table, C_s was calculated from Eq (18); ϵ' was calculated from the thickness x with the expression given on page 29; $\phi_{th} f_x$

was calculated by re-arrangement of Eq (23); and ϕ_{th} was taken as 1.193 times the original thermal flux in the standard graphite pile (see Appendix C). For clarity, the pertinent equations are reproduced below:

$$C_s = \frac{\lambda C_{net} e^{\lambda t_w}}{(1-e^{-\lambda t_e})(1-e^{-\lambda t_c})} \qquad (18)$$

$$\epsilon' = \exp[(-0.01045)x]$$

$$\phi_{th} f_x = \frac{1.128 AW}{\sigma_0 N_a} 1000 \left[\frac{C_s(b)}{\epsilon_b M_b} - \frac{F_{Cd} C_s(Cd)}{\epsilon_{Cd} M_{Cd}} \right] \qquad (23a)$$

A linear least squares of $\phi_{th} f_x$ vs ϕ_{th} from the above table gave f_x=(0.428±0.021) , to complete the efficiency term of the detector system.

Appendix F: Graphite Pile Fluxes

The data used for Table 2, Neutron Fluxes in Graphite Pile, are given here. Equation (23) was used to calculate the fluxes, using the value for f_x determined from Appendix E. The values used for these calculations are, as for all pertinent calculations, listed by count number in Appendix I. The values for ϕ_{in} in Table 2 are averages of the values below for each stringer location.

Cnt #	Str #	ϕ_{in}
16 19	1 1	3870 ± 210
64 82	1 1	3900 ± 210
13 22	2 2	7570 ± 390
67 85	2 2	8150 ± 420
10 25	3 3	9460 ± 480
70 88	3 3	9540 ± 490
7 28	4 4	6719 ± 340
73 91	4 4	7300 ± 370
4 31	5 5	3850 ± 200
76 94	5 5	3960 ± 200
1 34	6 6	1850 ± 100
79 97	6 6	1930 ± 100

Appendix G: Comparison of M580 and M1170 Outputs

This appendix describes the measures used to compare the output of neutron sources M1170 and M580. Their outputs were both measured on the same day. The setup was as in Figure 9. A helium-3 tube with a 2-inch cadmium cap to block direct neutrons was used in the long counter. The long counter was set on the edge of the Ping-pong table in the basement of Bldg 470. Parameters of the experiment are listed in Table 20.

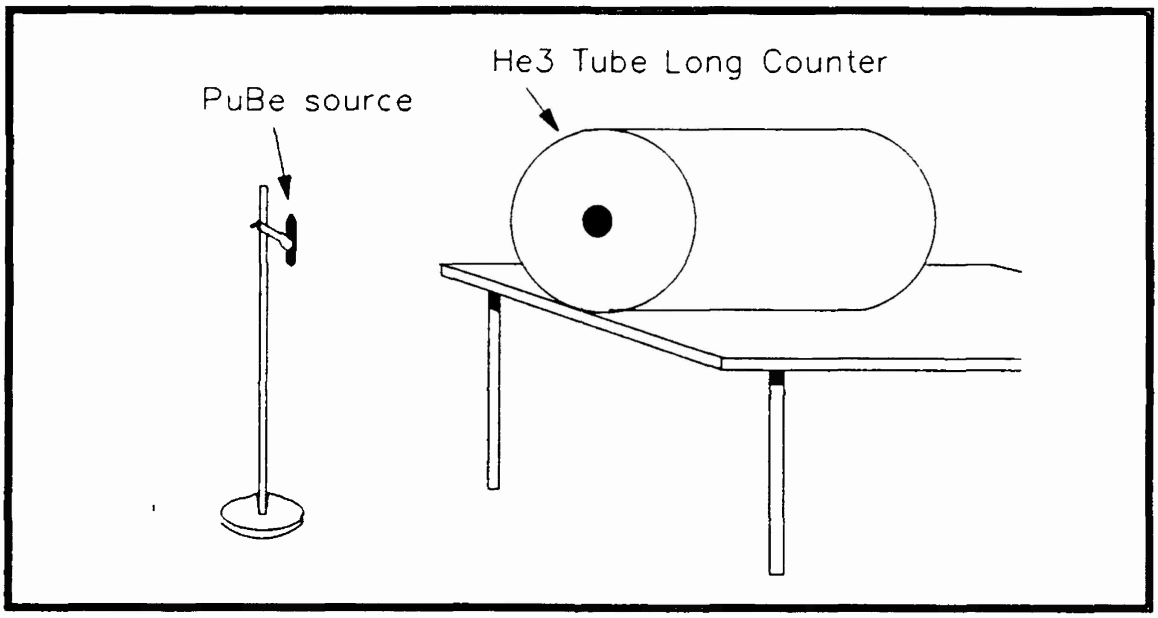

Figure 9 Setup for Comparison of M580 and M1170 Neutron Sources

Four counts of 100 seconds each were made with both sources. The results are listed in Table 21.

Table 20: M580 and M1170 Neutron Source Comparison Parameters:

Distance, source to He-3 tube:	2 meters
Height of source and counter:	94 cm
Long counter settings:	1200 volts

Table 21: M580 and M1170 Comparison

Trial	M580 Counts	M1170 Counts
1	34271	36459
2	33932	36422
3	34454	36471
4	34244	36419
Average:	34225 ± 217	36443 ± 26

The ratio of measured outputs is 1.0648 ± 0.0068 . The measurements were done on 31 Oct 89. On this date, t = 26.67 yrs for M1170 and t = 29.36 yrs for M580. The calculated values according to Eq. (33) are 1.1×10^7 n/s for M1170 and 1.06×10^7 n/s for M580 (using p_3=0.0044). The calculated ratio, then, is 1.04. This agrees reasonably well with the measured ratio, and confirms 0.0044 as the original ^{241}Pu fraction in M580.

Appendix H: Flux Integrator Calibration Constant

The value of the calibration constant K for the flux integrators, used in the equation $\phi = KS_a$, was obtained by linear least squares. The graph of the data was presented in section 4.3. This appendix describes the data and calculations used to obtain the calibration constant.

To calculate this value, one may let ϕ be the independent variable, or one may let S_a be the independent variable. Here S_a was plotted on the x-axis and ϕ along the y-axis to match the equation above. This assigns S_a as the independent value.

S_a was calculated as $A_a/Mass$, with A_a from Eq. (7). ϕ was determined by

$$\phi = \frac{Q(M1170)}{4}\pi r^2(1.15) \qquad (34)$$

where Q(M1170) is the output of PuBe source M1170, 1.15 is the anisotropy of M1170 (Rossano, 1989: 69), and ground scatter was accounted for by Eq (26).

The method of linear least squares was used. The equations after the table are from chapter six of Bevington. The following table gives the data and the statistical expressions used.

Table 22: Flux Integrator Calibration, I

Cnt #	i	$(S_- \pm \sigma)$ x 10^{-6} [Bq/mg]	ϕ $n/s-cm^2$	ϕ^2	$\phi S_- \pm \sigma$	$(S_-^2 \pm \sigma)$ x 10^{-3}	$a + b x_i$	Δ_i^2
302	1	3.44 ± 0.14	104	10816	3.58 ± 0.15	1.183 ± 0.096	109.39	29.05
303	2	4.91 ± 0.19	151	22801	7.41 ± 0.29	2.41 ± 0.19	153.04	4.16
304	3	4.80 ± 0.19	151	22801	7.25 ± 0.29	2.30 ± 0.18	149.77	1.51
305	4	3.23 ± 0.13	104	10816	3.36 ± 0.14	1.043 ± 0.084	103.16	0.71
306	5	3.29 ± 0.13	104	10816	3.42 ± 0.14	1.082 ± 0.085	104.94	0.88
332	6	3.82 ± 0.15	121	14641	4.62 ± 0.18	1.46 ± 0.11	120.68	0.10
333	7	3.72 ± 0.15	121	14641	4.50 ± 0.18	1.38 ± 0.11	117.71	10.82
334	8	3.42 ± 0.14	107	11449	3.66 ± 0.15	1.170 ± 0.096	108.80	3.24
335	9	3.21 ± 0.13	107	11449	3.43 ± 0.14	1.030 ± 0.042	102.56	19.71
Sum	N=9	33.84 ± 0.46	1070	130230	41.23 ± 0.58	13.06 ± 0.36		70.18

$$\Delta = N\sum\phi^2 - (\sum\phi)^2 = 0.00302544$$

$$a = \frac{\sum S_-^2 \sum\phi - \sum S_- \sum\phi S_-}{\Delta} = 7.26 \qquad b = \frac{N\sum\phi S_- - \sum S_- \sum\phi}{\Delta} = 2968.82$$

$$s^2 = \frac{1}{N-2}\sum(\Delta^2) = 10.026$$

$$\sigma_a^2 = \frac{s^2\sum S_-^2}{\Delta} = 43.28 \quad \textit{so that} \quad \sigma_a = 6.58$$

$$\sigma_b^2 = \frac{Ns^2}{\Delta} = 29825 \quad \textit{so that} \quad \sigma_b = 173$$

These equations give

$$\phi = (2970 \pm 170) S_{\infty} + (7.3 \pm 6.6) \qquad (28)$$

for the relation between flux and saturation activity. This is in agreement with Rossano's results, though the uncertainties are larger than his.

The uncertainties of the data are given in the table, but they are not used to calculate the final uncertainly in the activity-to-flux equation. The uncertainties were first calulated using propogation of error, as outlined in Bevington. However, the uncertainties obtained were not believable as calculated; the uncertainty in K was found to be about 3/4 of the value of K itself. If one were to calculate K for each data point, the individual uncertainties were never more than about 5% of the value of K. Either the uncertainties by propogation of errors blew up by this stage in the calculations, or they were misapplied. At any rate it was decided to use the uncertainties given here, based on the statistical method used to calculate K from ϕ and S_{∞}. They gave much more believable results.

If ϕ were used as the independent variable, so that ϕ is plotted along the x-axis and S_{∞} along the y-axis, the last two columns of the table above and all the equations that follow will change. For comparison, they are given here.

Table 23: Flux Integrator Calibration, II

Cnt #	i	$a + b x_i$	Δ_i^2
302	1	0.0327	2.89×10^{-6}
303	2	0.0482	8.1×10^{-7}
304	3	0.0482	4.0×10^{-8}
305	4	0.0327	1.6×10^{-7}
306	5	0.0327	4.0×10^{-8}
332	6	0.0383	1.0×10^{-8}
333	7	0.0383	1.21×10^{-6}
334	8	0.0337	2.5×10^{-7}
335	9	0.0337	2.56×10^{-6}

Done this way, the equations give these results:

$$\Delta = N\sum\phi^2 - (\sum\phi)^2 = 27170$$

$$a = \frac{\sum S_-^2 \sum\phi - \sum S_- \sum\phi S_-}{\Delta} = -0.0017 \qquad b = \frac{N\sum\phi S_- - \sum S_- \sum\phi}{\Delta} = 3.30585 \times 10^{-4}$$

$$s^2 = \frac{1}{N-2}\sum(\Delta^2) = 1.139 \times 10^{-6}$$

$$\sigma_a^2 = \frac{s^2 \sum S_-^2}{\Delta} = 5.46 \times 10^{-6} \qquad \textit{so that} \qquad \sigma_a = 2.34 \times 10^{-3}$$

$$\sigma_b^2 = \frac{N s^2}{\Delta} = 3.77 \times 10^{-7} \qquad \textit{so that} \qquad \sigma_b = 1.94 \times 10^{-5}$$

Under this arrangement, $K = 1/b = 3025 \pm 178$, if the appropriate terms are inverted. The uncertainty in the intercept is greater than the intercept itself, so again the intercept may be interpreted as zero. Statistically the answer is not different from the previous one; and based on the experiment used ϕ may be more the independent variable than S_- . This arrangement was used by a previous researcher (Rossano, 1988:

37-39). However, this researcher chose to use the first arrangement given above in his calculations; it seemed to be the more direct method to reach the desired equation. Incidentally it also gives the same answer as in the previous work on this topic (Rossano, 1988: 38), though it was not chosen specifically for this reason.

Appendix I: Foil Counting Data

The following list includes most of the pertinent irradiation data from each foil measurement done in preparation for this thesis. The count number is simply an arbitrary designator for each individual count of irradiated foils. The foil numbers are those given in the previous section. $C(t_c)$ refers to the gross (or total) counts in counting time t_c; no correction for background counts are included in that column. t_e is the foil exposure time, and t_w is the waiting time between end of irradiation and beginning of counting. r_{bg} is the background count rate for the particular detector used, as measured by background count data for some time within a few days of the particular count. All counting was done with the G-M detector with a silver backscatterer. It was located in Building 470, in the lab rooms.

Count Number	Foil Number	$C(t_c)$	t_c [s]	r_{bg} [s^{-1}]	t_e [m]	t_w [m]
1	40	3110	400	0.2772	1404	7
4	41	6287	400	0.2772	1345	40
7	42	13815	400	0.2772	1396	15
10	43	20692	400	0.2772	1301	19
13	44	20082	400	0.2772	1340	29
16	45	9244	400	0.2772	1302	3
19	46	6987	800	0.2772	1308	52
22	47	9323	500	0.2772	1255	20
25	48	6751	400	0.2772	1254	9
28	49	5578	800	0.2772	1307	32
31	50	1582	1000	0.2772	1380	4

Count Number	Foil Number	$C(t_c)$	t_c [s]	r_{bg} [s^{-1}]	t_e [m]	t_w [m]
34	51	485	1000	0.2772	1381	23
36	37	7535	500	0.2772	1370	20
64	22	6371	400	0.2772	2929	5765
67	23	13170	400	0.2772	2933	5781
70	24	14512	400	0.2772	2968	5749
73	25	9145	400	0.2772	2967	5743
76	26	6487	600	0.2772	2895	5852
79	27	3096	600	0.2772	2895	5865
82	31	3164	100	0.2772	9917	37
85	32	6916	100	0.2772	9919	24
88	33	6397	100	0.2772	9920	47
91	34	2303	100	0.2772	9922	37
94	35	2622	500	0.2772	9923	48
97	36	1139	1000	0.2772	9923	68
141	36	2566	1000	0.284	0.83	214 ± 10
142	38	1974	1000	0.284	0.83	233 ± 10
143	42	2048	1000	0.284	0.85	245 ± 10
144	40	1934	1000	0.284	0.85	285 ± 10
145	35	2126	1000	0.284	0.83	273 ± 10
146	45	2092	1000	0.284	0.83	283 ± 10
147	39	1500	1000	0.284	0.83	311 ± 10
148	44	2038	1000	0.284	0.83	320 ± 10
149	46	3228	1000	0.303	0.92	505
150	47	1412	1000	0.303	0.64	503
151	48	2152	1000	0.303	2.17	447

Count Number	Foil Number	$C(t_c)$	t_c [s]	r_{bg} [s^{-1}]	t_e [m]	t_w [m]
152	49	3151	1000	0.303	0.80	443
253	J-08	10175	500	0.320	2875	8
254	J-08	10056	500	0.320	2875	20
255	J-08	9996	500	0.320	2875	29
256	J-08	10082	500	0.320	2875	40
257	J-09	10062	500	0.320	2875	51
258	J-09	9174	600	0.320	2875	1699
259	J-09	10192	500	0.320	2875	61
260	J-10	10041	500	0.320	2875	72
261	J-10	7652	500	0.320	2875	1678
262	J-10	8961	600	0.320	2875	1688
263	J-11	9874	500	0.320	2875	255
264	J-11	9811	500	0.320	2875	264
265	J-11	9789	500	0.320	2875	274
266	J-08, J-09	14553	500	0.320	2875	285
267	J-08, J-09	11481	500	0.320	2875	1712
268	J-10, J-09, J-08	17021	500	0.320	2875	297
269	J-10, J-09, J-08	13567	500	0.320	2875	1724
270	J-11, J-10, J-09, J-08	18973	500	0.320	2875	311

Count Number	Foil Number	$C(t_c)$	t_c [s]	r_{bg} [s^{-1}]	t_e [m]	t_w [m]
271	J-11, J-10, J-09, J-08	19017	500	0.320	2875	320
272	J-10, J-11	14375	500	0.320	2875	331
273	J-10, J-11	11352	500	0.320	2875	1755
274	J-09, J-10, J-11	16974	500	0.320	2875	341
275	J-09, J-10, J-11	13500	500	0.320	2875	1744
276	J-08, J-09, J-10, J-11	18895	500	0.320	2875	351
277	J-08, J-09, J-10, J-11	14930	500	0.320	2875	1735
298	26	8214	4000	0.319	1.78	165
299	31	10537	5000	0.319	0.75	163
300	33	6985	5000	0.319	0.82	243
301	34	8754	6000	0.319	0.68	75 ± 5
302	25	10654	10000	0.321	2382	29
303	37	11831	10000	0.3219	1804	56
304	43	11359	10000	0.3219	1804	226
305	35	13370	10000	0.325	3891	18
306	36	13997	10000	0.325	3891	208
307	38	12037	6000	0.324	0.63	107
308	39	12298	8000	0.324	0.83	214

Count Number	Foil Number	$C(t_c)$	t_c [s]	r_{bg} [s^{-1}]	t_e [m]	t_w [m]
309	40	12226	8000	0.324	0.70	332 ± 5
310	51	2644	1000	0.335	1	313
311	32	10774	5000	0.335	1	1477
312	23	11326	5000	0.335	1	1388
313	24	2779	1000	0.335	1	323
314	27	12961	5000	0.335	1	660
315	30	9246	4000	0.335	1	1285
316	44	2671	1000	0.335	1	326
317	42	9919	4000	0.335	1	1034
318	53	2858	1000	0.335	1	334
319	45	10185	4000	0.335	1	1079
320	55	14959	1000	0.335	6	312
321	54	6350	1000	0.335	6	343
322	52	5251	1000	0.335	6	363
323	56	3032	1000	0.335	6	382
324	58	14624	1000	0.335	6	470
325	57	6809	1000	0.335	6	488
326	62	5313	1000	0.335	6	527
327	63	2423	1000	0.335	6	546
328	59	15219	1000	0.335	6	373
329	60	6942	1000	0.335	6	399
330	61	5761	1000	0.335	6	419
331	64	2589	1000	0.335	6	437

Count Number	Foil Number	$C(t_c)$	t_c [s]	r_{bg} [s^{-1}]	t_e [m]	t_w [m]
332	71	12065	10000	0.331	2350	25
333	74	11439	10000	0.331	2350	474
334	65	11176	12000	0.338	1619	64
335	66	15533	18000	0.338	1619	269
336	68	11572	1000	0.342	3	177
337	67	8558	1000	0.342	3	305
338	69	11731	1200	0.342	3	325
339	70	7165	1200	0.342	3	248
340	83	12368	1200	0.342	3	396
341	84	9462	1200	0.342	3	419
342	72	13481	1200	0.342	3	430
343	73	14311	1800	0.342	3	452
344	75	11766	1200	0.342	3	475
345	76	10222	1800	0.342	3	499
346	79	13349	1200	0.342	3	488
347	80	14249	1800	0.342	3	510
348	78	11037	1200	0.342	3	562
349	77	10086	1800	0.342	3	585
350	46	5946	1200	0.327	6.18	435
351	47	4841	1200	0.327	6.18	457
352	48	3524	1200	0.327	6.18	470
353	49	5872	1200	0.327	6.18	491
354	40	3792	1200	0.327	6.18	516
355	38	6222	1200	0.327	6.48	538

Count Number	Foil Number	$C(t_c)$	t_c [s]	r_{bg} [s^{-1}]	t_e [m]	t_w [m]
356	39	2682	1800	0.327	6.48	1052
357	41	1432	1800	0.327	6.48	1083
358	25	6215	1800	0.327	6.18	1120
359	22	7219	1800	0.327	6.18	1152
360	50	2507	1800	0.327	6.18	1184
361	24	1477	1800	0.327	6.18	1216
362	26	5945	1200	0.327	6.18	1248
363	31	4179	1200	0.327	6.18	1272
364	51	2378	1800	0.327	6.18	1295
365	44	1365	1800	0.327	6.18	1329
366	33	5246	1200	0.327	6.18	1350
367	34	2868	1200	0.327	6.18	1371
368	27	2307	1800	0.327	6.18	1394
369	42	1409	1800	0.327	6.18	1438
370	37	5776	1200	0.327	6.18	1459
371	43	3865	1200	0.327	6.18	1483
372	45	2290	1800	0.327	6.18	1504
373	23	1377	1800	0.327	6.18	1535
374	32	4735	1200	0.327	6.18	1557
375	35	4043	1800	0.327	6.18	1583
376	36	2257	1800	0.327	6.18	1616
377	30	1317	1800	0.327	6.18	1648

Bibliography

Anderson, M. Edward. "Increases in Neutron Yields of Plutonium-Berylium (α-n) Sources," Nuclear Applications,4,: 142-147 (March 1968).

-----. "Increases in Neutron Yields of Pu239-Be Neutron Sources-II," Nuclear Technology, 52: 428-430 (March 1981).

Attix, Frank H. Introduction to Radiological Physics and Radiation Dosimetry, pp. 463-524. John Wiley and Sons, New York, 1969.

Bevington, Philip R. Data Reduction and Error Analysis for the Physical Sciences. McGraw-Hill Book Company, 1969.

Bruninx, E. "The Measurement of Fast Neutron Flux Densities Above 0.5 MeV by a Simple Moderation Method," International Journal of Applied Radiation and Isotopes, 21: 657-666 (1970).

Burden, Richard L. and J. Douglas Faires. Numerical Analysis, 3rd Ed., pp. 362-369. Prindle, Weber & Schmidt, 1985.

Garber, D.I. and R.R. Kinsey. Neutron Cross Sections, Volume II, Curves. Brookhaven National Laboratory, January 1976.

Greenfield, Moses A., Roscoe L. Koontz, Alan A. Jarrett, and Juanita K. Taylor. "Measuring Flux Absolutely With Indium Foils," Nucleonics, 15(3): 57-61 (March 1957).

Jenkins, T.M. "Simple Recipes for Ground Scattering in Neutron Detector Calibration," Health Physics, 39: 41-47 (July 1980).

Knoll, Glenn F. Radiation Detection and Measurement. John Wiley and Sons, New York, 1979.

Martin, D. H. "Correction Factors for Cd-Covered-Foil Measurements," Nucleonics, 13(3): 52-53 (March 1955).

McCall, R.C. and W.P. Swanson. "Neutron Sources and Their Characteristics," National Bureau of Standards SP 554: 75-86 (1979).

McGinley, P.H., M. Wood, M. Mills, and R. Rodriguez. "Dose Levels Due to Neutrons in the Vicinity of High-Energy Medical Accelerators," Medical Physics, 3(6): 397-402 (November/December 1976).

Mound Laboratory. Shipping Data - Plutonium Neutron Source. Neutron Source No. M580. Monsanto Research Corporation, June 1960.

Mound Laboratory. Shipping Data - Plutonium Neutron Source. Neutron Source No. M1170. Monsanto Research Corporation, 9 March 1962.

Nath, Ravinder, Edward R. Epp, John S. Laughlin, William P. Swanson, and Victor P. Bond. "Neutrons from High-Energy X-ray Medical Accelerators: An Estimate of Risk to the Radiotherapy Patient," Medical Physics, 11(3): 231-241 (May/June 1984).

NCRP Report No. 31. Shielding for High Energy Electron Accelerator Installations. National Council on Radiation Protection and Measurements, Bethesda, MD, 1 July 1964.

NCRP Report No. 58. A Handbook of Radioactivity Measurements Procedures, 2nd ed. National Council on Radiation Protection and Measurements, Bethesda, MD, 1 February 1985.

NCRP Report No. 79. Neutron Contamination from Medical Electron Accelerators. National Council on Radiation Protection and Measurements, Bethesda, MD, 1 November 1984.

Price, William J. Nuclear Radiation Detection (2nd Edition). New York: McGraw-Hill Book Company, 1964.

Purdy, James A. and Glenn P. Glasgow. "Neutron Leakage Around a 20-MeV (18-MV x Ray) Linac with a Modified Neutron Shield," Health Physics, 46(3): 669-674 (March 1984).

Reactor Experiments Inc. Neutron Flux Integrator. San Carlos, CA, undated.

Rossano, Mark J. Flux and Spectrum of Neutrons Generated from 25 MV Medical X-Ray Therapy Machine. AFIT/GNE/ENP/89J-1 MS Thesis. May 1989.

Sanders, M.E., Dave, A.L. and McGinley, P.H. "Photoneutron Contirbution from the Thermal Neutron Shield in a Typical Activation Foil Neutron Detector Exposed to a 33-MV x-ray Beam," Health Physics, 47(1): 107-109 (July 1984).

Stanford, George S. and James H. Seckinger. Thickness Corrections for Neutron-Activated Gold Foils. ANL-7545. Argonne National Laboratory. Argonne, IL, February 1969.

WADD-TR-61-174. AF NETF Graphite Standard Pile. Nuclear Engineering Test Facility, Directorate of Engineering Test, Aeronautical Systems Division, Air Force Systems Command, Wright-Patterson AFB, OH, March 1962.

Walker, William F. et al. Chart of the Nuclides. General Electric Company - Nuclear Energy Operations, San Jose, CA, 1984.

Wilenzick, R.M., P.R. Almond, G.D. Oliver, Jr., and C.E. de Almeida. "Measurement of Fast Neutrons Produced by High-Energy X-ray Beams of Medical Electron Accelerators," Phys. Med. Biol., 18(3): 396-408 (1973).

Vita

Captain Richard A. Jackson, USAF, [redacted]. He graduated with honors from Coosa High School in 1979. In 1983 he graduated cum laude from Berry College, Mt. Berry, GA, with a B.A. in Physics. Following his baccalaureate he spent two years studying atmospheric science at Colorado State University, Fort Collins, CO. In 1985 he joined the Air Force as a scientific officer. Graduating from OTS in August, 1985, he was assigned to Air Force Global Weather Central, Offutt AFB, NE, where he maintained computer software for space forecasting operations. He entered AFIT in September, 1988. His following assignment was as a nuclear materials analysis at Technical Operations Division, McClellan AFB, CA, supporting the nuclear test ban treaties.

Permanent address: 6 Oreburg Rd, NW
Rome, Georgia 30161

AFIT/GNE/ENP/92J-01

NEUTRON FLUENCE AND DOSE FROM A VARIAN CLINAC 1800 ACCELERATOR

THESIS

Richard A. Jackson
Captain, USAF

AFIT/GNE/ENP/92J-01

AFIT/GNE/ENP/92J-01

NEUTRON FLUENCE AND DOSE FROM A VARIAN CLINAC 1800 ACCELERATOR

THESIS

Presented to the Faculty of the School of Engineering
of the Air Force Institue of Technology
Air University
in Partial Fulfillment of the
Requirements for the Degree of
Master of Science in Nuclear Science

Richard A. Jackson
Captain, USAF

November 1991

REPORT DOCUMENTATION PAGE

Form Approved
OMB No. 0704-0188

1. AGENCY USE ONLY *(Leave blank)*	2. REPORT DATE	3. REPORT TYPE AND DATES COVERED
	Jun 92	Thesis

4. TITLE AND SUBTITLE
NEUTRON FLUENCE AND DOSE FROM A VARIAN CLINIC 1800 ACCELERATOR

5. FUNDING NUMBERS

6. AUTHOR(S)
CAPT RICHARD A. JACKSON

7. PERFORMING ORGANIZATION NAME(S) AND ADDRESS(ES)
AFIT/ENP

8. PERFORMING ORGANIZATION REPORT NUMBER
AFIT/GNE/ENP/92J-01

9. SPONSORING/MONITORING AGENCY NAME(S) AND ADDRESS(ES)

10. SPONSORING/MONITORING AGENCY REPORT NUMBER

11. SUPPLEMENTARY NOTES

12a. DISTRIBUTION/AVAILABILITY STATEMENT
Unlimited

12b. DISTRIBUTION CODE

13. ABSTRACT *(Maximum 200 words)*

The goals of this study were (1) to verify calibration factors determined by previous experiment for relating counts from activated gold foils to neutron fluences, and (2) to use the method to determine neutron fluences under various operating conditions of the Varian Clinac 1800 (18-MeV) electron accelerator at the WPAFB Medical Center. For comparison similar measurements were made of the CGM Saturne 1 at Kettering Memorial Hospital, Dayton OH.

14. SUBJECT TERMS	15. NUMBER OF PAGES
	16. PRICE CODE

17. SECURITY CLASSIFICATION OF REPORT	18. SECURITY CLASSIFICATION OF THIS PAGE	19. SECURITY CLASSIFICATION OF ABSTRACT	20. LIMITATION OF ABSTRACT
Unclas	Unclas	Unclas	Unlimited